Cell

Volume 159
Number 4

November 6, 2014

www.cell.com

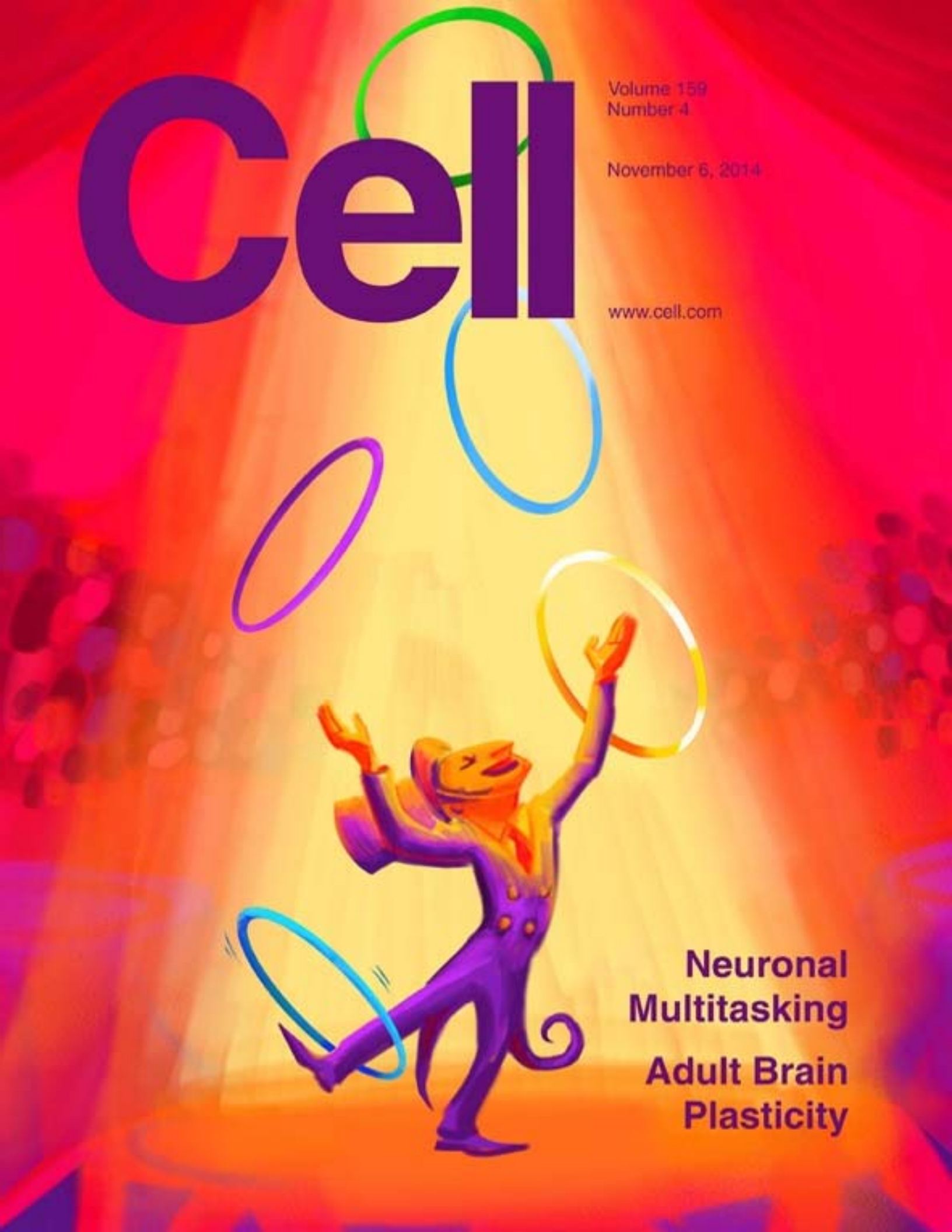

Neuronal Multitasking

Adult Brain Plasticity

Cell

Encoding of Both Analog- and Digital-like Behavioral Outputs by One *C. elegans* Interneuron

Zhaoyu Li,[1] Jie Liu,[1] Maohua Zheng,[1] and X.Z. Shawn Xu[1,*]
[1]Life Sciences Institute and Department of Molecular and Integrative Physiology, University of Michigan, Ann Arbor, MI 48109, USA
*Correspondence: shawnxu@umich.edu
http://dx.doi.org/10.1016/j.cell.2014.09.056

SUMMARY

Model organisms usually possess a small nervous system but nevertheless execute a large array of complex behaviors, suggesting that some neurons are likely multifunctional and may encode multiple behavioral outputs. Here, we show that the *C. elegans* interneuron AIY regulates two distinct behavioral outputs: locomotion speed and direction-switch by recruiting two different circuits. The "speed" circuit is excitatory with a wide dynamic range, which is well suited to encode speed, an analog-like output. The "direction-switch" circuit is inhibitory with a narrow dynamic range, which is ideal for encoding direction-switch, a digital-like output. Both circuits employ the neurotransmitter ACh but utilize distinct postsynaptic ACh receptors, whose distinct biophysical properties contribute to the distinct dynamic ranges of the two circuits. This mechanism enables graded *C. elegans* synapses to encode both analog- and digital-like outputs. Our studies illustrate how an interneuron in a simple organism encodes multiple behavioral outputs at the circuit, synaptic, and molecular levels.

INTRODUCTION

How the nervous system and genes generate behavior is one of the most fundamental questions in neuroscience. Unlike the human brain with billions of neurons, lower organisms such as *Caenorhabditis elegans*, *Drosophila*, crustaceans, mollusks, and zebrafish possess a much smaller nervous system and are therefore widely used as models to study the neural and genetic control of behavior. Although equipped with a small nervous system, these model organisms are capable of performing a diverse range of complex behaviors, many of which are analogous to those manifested by humans (Berkowitz et al., 2010; de Bono and Maricq, 2005; Sokolowski, 2001). This suggests that neurons in these organisms may not all be specialized and some may regulate multiple behavioral outputs (Berkowitz et al., 2010; Briggman and Kristan, 2008). Interestingly, this phenomenon is not restricted to simple model organisms, as many neurons in the mammalian brain, especially in the cortex, also have multifunctional properties (Jankowska, 2001; Schiller, 1996). However, how single neurons encode multiple behavioral outputs is not well understood.

As the nematode *C. elegans* represents the only organism whose connectome has been reconstructed by electron microscopy, it has emerged as a popular model for dissecting the neural and genetic basis of behavior at the single neuron resolution (de Bono and Maricq, 2005). *C. elegans* has a very small nervous system with merely 302 neurons. Despite this simplicity, worms execute a broad spectrum of behaviors, ranging from motor and sensory behaviors to the more complex mating, social, sleep, and drug-dependent behaviors, as well as associative learning and memory (de Bono and Maricq, 2005; de Bono et al., 2002; Feng et al., 2006; Liu and Sternberg, 1995; Raizen et al., 2008). This large repertoire of complex behaviors places a high demand on the functionality of the worm nervous system. As such, many worm neurons are thought to be multifunctional (Bargmann, 2012; de Bono and Maricq, 2005). This notion, however, provokes some intriguing questions. First, what are the circuit and synaptic mechanisms by which single neurons encode multiple behavioral outputs? Additionally, similar to many types of synapses in mammalian sensory organs, most, if not all, *C. elegans* synapses are believed to be graded; yet some worm behavioral outputs are manifested in an all-or-none digital-like fashion (Bargmann and Marder, 2013; Goodman et al., 1998; Liu et al., 2009). This raises the question: how could graded synapses encode digital-like behavioral outputs?

Here, we investigated these questions in *C. elegans* using a multifaceted approach by integrating calcium imaging, optogenetics, molecular genetics, laser ablation, and electrophysiology at the single neuron resolution. By characterizing a model interneuron AIY that regulates both analog- and digital-like behavioral outputs, we show that at the circuit level, one strategy for a neuron to control multiple behavioral outputs is to recruit multiple downstream circuits with each regulating a specific behavioral output. At the synaptic level, we show that worm synapses display distinct dynamic ranges, which contributes to their ability to encode both analog- and digital-like behavioral outputs. At the molecular level, we demonstrate that the biophysical properties of postsynaptic receptors contribute to the distinct dynamic ranges of the synapses. These results reveal a mechanism by which graded *C. elegans* synapses encode both analog- and digital-like behavioral outputs. Our studies define the circuit,

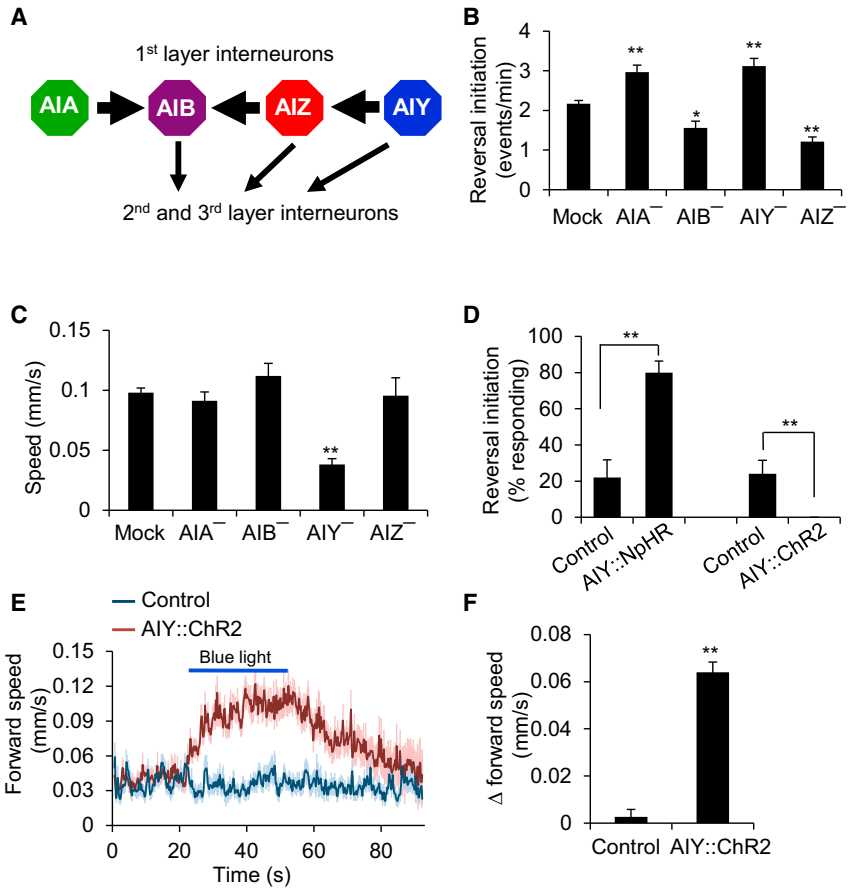

Figure 1. AIY Regulates Locomotion Speed and Direction-Switch

(A) Schematic showing the connectivity of the first layer interneurons.

(B) Laser ablation. n ≥ 5. *p < 0.03; **p < 0.0005 (ANOVA with Tukey's HSD test).

(C) Laser ablation shows that AIY is important for locomotion speed. n ≥ 5. **p < 0.0001 (ANOVA with Tukey's HSD test).

(D) Optogenetic inhibition or stimulation of AIY promotes or suppress reversal initiation, respectively. Worms expressing NpHR or ChR2 as a transgene specifically in AIY were tested for reversal initiation triggered by yellow or blue light (5 s pulse). Control: nontransgenic siblings (a similar control result was obtained by assaying the transgenic animals reared on retinal-free plates). The low level of reversal events in the control resulted from spontaneous reversals. n = 5. **p < 0.0001 (t test).

(E and F) Optogenetic stimulation of AIY promotes locomotion speed. Worms expressing ChR2 as a transgene specifically in AIY were tested under blue light (30 s pulse). Control: nontransgenic siblings. (E) Forward speed traces. The shades along the traces represent error bars. For clarity, the very few reversal events were removed. (F) Bar graph. n ≥ 22. **p < 0.0001 (t test).

All error bars represent SEM. See also Figure S1.

synaptic, and molecular mechanisms by which an interneuron encodes multiple behavioral outputs in a genetic model organism.

RESULTS

The Interneuron AIY Regulates Two Distinct Behavioral Outputs

We focused on locomotion behavior, one of the most prominent behaviors in *C. elegans* (Piggott et al., 2011; Tsalik and Hobert, 2003; Zheng et al., 1999). Locomotion forms the foundation of most, if not all worm behaviors (e.g., motor, sensory, social, mating, sleep, etc.), as these behaviors are, to varying degrees, all manifested at the locomotion level. During locomotion, worms spend most of their time moving forward and occasionally change locomotion direction by switching to backward movement (reversal) (Piggott et al., 2011; Zheng et al., 1999). We recorded locomotion behavior using an automated worm tracking system (Feng et al., 2006) and quantified two simple parameters: speed and reversal initiation. These two parameters represent two distinct motor outputs, with the former reporting the overall activity of locomotion and the latter describing the direction-switch of locomotion. They also bear another distinction in that speed is intrinsically an analog-like parameter, whereas reversal occurs in an all-or-none fashion and thus represents a digital-like output.

As a first step, we sought to identify a neuron that regulates these two behavioral outputs. This would offer us an opportunity to dissect the mechanisms underlying encoding of two distinct behavioral outputs by one neuron. Interneurons are known to play a pivotal role in controlling locomotion, particularly spontaneous locomotion (Gray et al., 2005). Based on the wiring diagram, they are organized in a hierarchy-like pattern and send outputs to motor neurons that drive locomotion (Gray et al., 2005). We focused our initial attention on the 1st layer interneurons (i.e., AIA, AIB, AIZ, and AIY), as they remain at the very top of the interneuron circuitry (Gray et al., 2005) (Figure 1A). Laser ablation of these four interneurons all affected reversal frequency (Figure 1B), consistent with previous reports (Chalasani et al., 2007; Gray et al., 2005; Kocabas et al., 2012; Tsalik and Hobert, 2003). Among them, AIY is particularly interesting, as loss of AIY led to a significant defect in both locomotion speed and reversal frequency (Figures 1B and 1C). Specifically, ablation of AIY reduced the speed of locomotion while increasing the frequency of reversals (Figures 1B and 1C). This suggests that while AIY promotes locomotion speed, it also suppresses the initiation of reversals. Thus, AIY likely regulates both locomotion speed and direction-switch.

If AIY regulates both speed and direction-switch as suggested by laser ablation, acute interrogation of AIY activity should affect both behavioral outputs. To test this, we took an optogenetic approach by expressing ChR2 and NpHR specifically in AIY as a transgene (Zhang et al., 2007). Transient inhibition of AIY activity by NpHR triggered reversals and suppressed locomotion

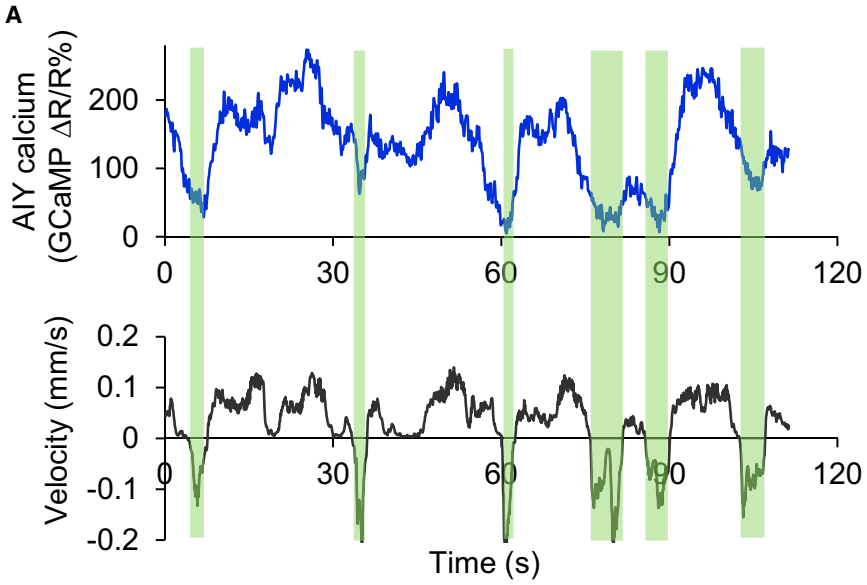

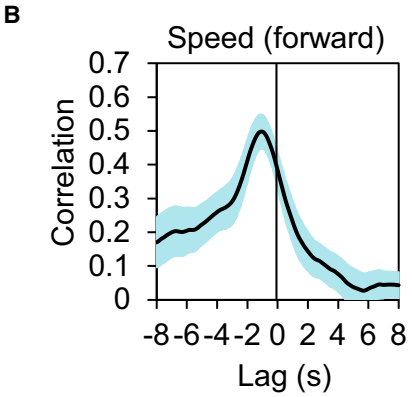

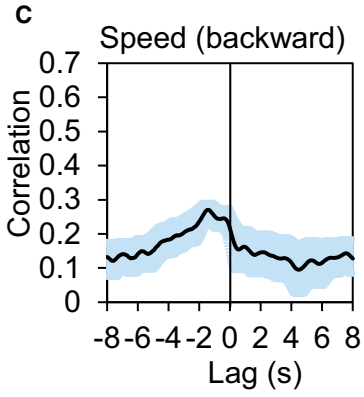

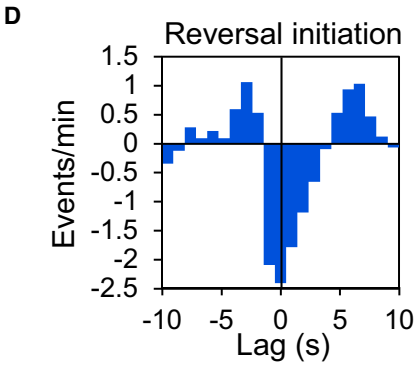

Figure 2. The Calcium Activity Pattern of AIY Correlates with Locomotion Speed and Direction-Switch in Freely Behaving Worms

(A) Calcium and locomotion velocity traces acquired with the CARIBN system. The windows highlighted in green denote reversals.

(B and C) Cross-correlation analysis shows that AIY calcium activity correlates with forward but not backward locomotion speed. The shades along the curves represent error bars (SEM). n = 8.

(D) Cross-correlogram showing that reversal initiation correlates with AIY activity decrease. Because reversal initiation occurs in an all-or-none fashion, cross-correlogram was used to analyze correlation using a method similar to that reported previously (Brown et al., 2004). The occurrence of a reversal event and the decrease/increase in calcium level at a given time point were analyzed for correlation. A negative value indicates that a reversal event coincided with a decrease in calcium level and vice versa.

See also Figure S2 and Movie S1.

speed (Figure 1D and Figures S1A and S1B available online), while activation of AIY by ChR2 suppressed the initiation of spontaneous reversals and stimulated locomotion speed (Figures 1D–1F). Prolonged optogenetic inhibition and stimulation of AIY also promoted and suppressed the initiation of spontaneous reversals, respectively (Figure S1C). The optogenetic data are more robust than those from laser ablation, probably because optogenetics tests the acute effects while laser ablation reports the chronic outcome, in which case animals may develop compensatory and adaptive mechanisms. Nevertheless, these two types of data together strongly suggest that AIY regulates both locomotion speed and direction-switch.

The Activity Pattern of AIY Correlates with Both Locomotion Speed and Direction-Switch in Freely Behaving Animals

While the data from both laser ablation and optogenetic interrogation strongly support a role for AIY in regulating locomotion speed and direction-switch, both approaches relied on the manipulation of AIY function and thus may not necessarily reveal exactly how AIY acts under native conditions. If AIY truly modulates locomotion speed and direction-switch, then the activity of AIY should correlate with these two behavioral outputs during locomotion. To address this question, we simultaneously recorded the activity of AIY and locomotion behavior in freely behaving worms using our calcium ratiometric imaging of behaving nematodes (CARIBN) system (Piggott et al., 2011). Notably, the calcium transients in AIY paralleled the speed of forward locomotion of the animal (Figure 2A; Movie S1). In addition, when the animal switched to backward movement (reversal), we observed a sharp decrease in AIY calcium level (Figures 2A and S2; Movie S1). This suggests that the activity of AIY may correlate with both locomotion speed and direction-switch. Indeed, cross-correlation analysis revealed

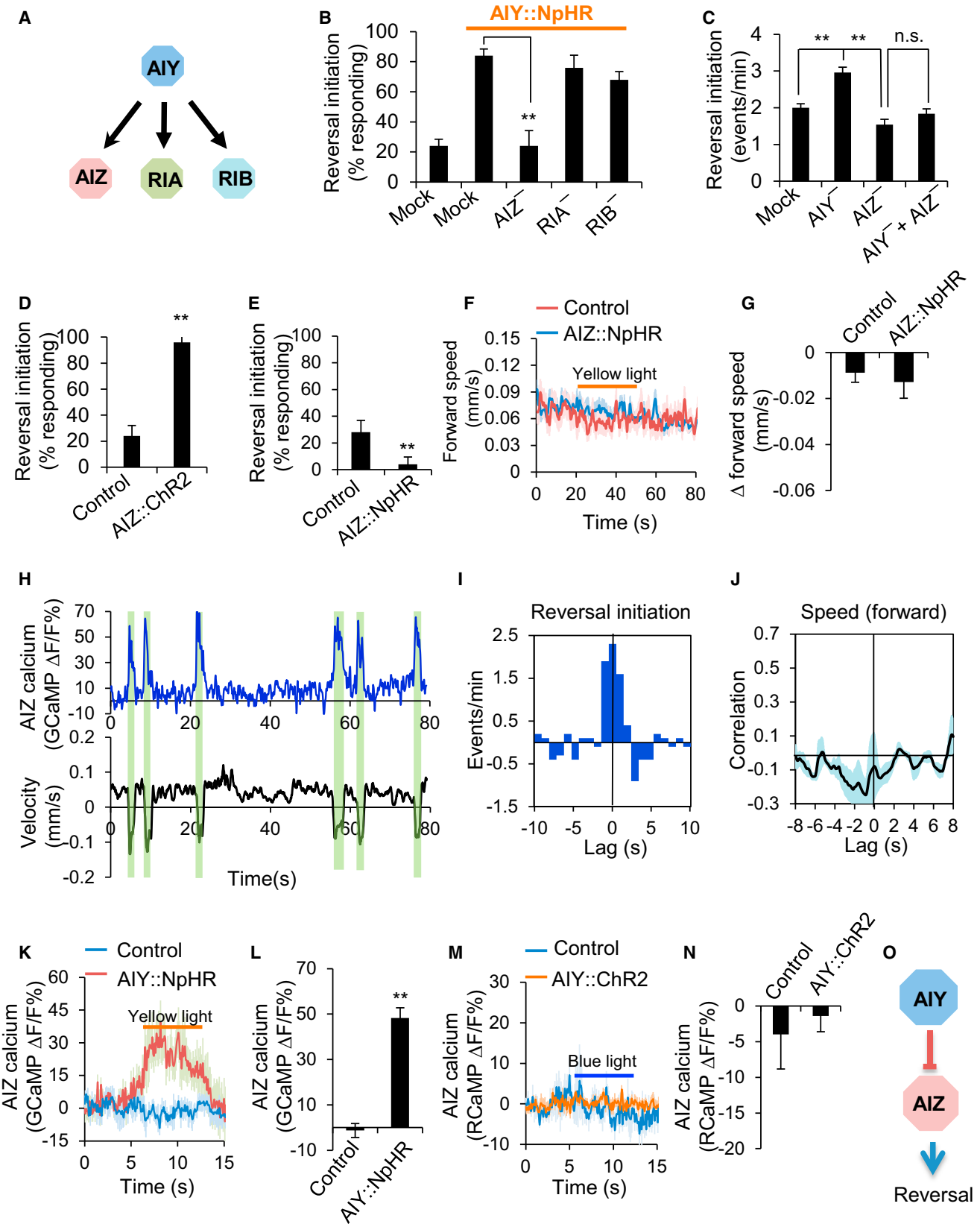

(legend on next page)

that AIY activity nicely correlated with forward locomotion speed (but not backward speed) (Figures 2B and 2C). In addition, cross-correlogram detected a strong correlation between the activity of AIY and the initiation of reversals (Figure 2D). Thus, the activity pattern of AIY appears to correlate with both locomotion speed and direction-switch, further supporting that AIY regulates these two motor outputs.

AIY Regulates Direction-Switch by Forming an Inhibitory Circuit with AIZ

Then how does AIY regulate locomotion speed and direction-switch? To approach this question, we set out to identify the neurons that act downstream of AIY to regulate these two behavioral outputs. Based on the wiring diagram, AIZ, RIA, and RIB are the primary downstream interneurons to which AIY sends synaptic outputs (Figure 3A). We thus ablated AIZ, RIA, and RIB and assayed whether and how this operation may affect the ability of AIY to regulate locomotion speed and direction-switch. We first examined direction-switch. Laser ablation of AIZ, but not RIA or RIB, abolished the ability of AIY (NpHR) to trigger reversals (Figure 3B). Thus, AIZ is required for AIY to regulate direction-switch, suggesting that AIZ acts downstream of AIY. Additional evidence came from spontaneous locomotion behavior: while ablation of AIY led to an increase in reversal frequency, simultaneous ablation of AIZ and AIY fully suppressed this hyperreversal phenotype (Figure 3C), further suggesting that AIZ acts downstream of AIY.

If AIZ acts downstream of AIY, this neuron should also regulate direction-switch. The observation that laser ablation of AIZ reduced reversal frequency is consistent with this view (Figure 3C). This data also suggests that AIZ promotes direction-switch. To provide further evidence, we optogenetically interrogated the role of AIZ in direction-switch by expressing ChR2 and NpHR as a transgene specifically in AIZ. Stimulation of AIZ by ChR2 triggered reversals (Figure 3D), while inhibition of AIZ by NpHR did not and instead suppressed spontaneous reversal frequency (Figure 3E), suggesting that AIZ promotes direction-switch. Notably, inhibition of AIZ by NpHR did not affect locomotion speed (Figures 3F and 3G), revealing a specific role for AIZ in regulating direction-switch. Thus, both laser ablation and optogenetic studies support that AIZ promotes direction-switch.

To obtain further evidence supporting a role for AIZ in direction-switch, we imaged the activity of AIZ in freely behaving worms using the CARIBN system. We found that AIZ increased its activity when worms initiated reversals (Figure 3H). Interestingly, though AIZ activity tightly correlated with reversal initiation (Figure 3I), no strong correlation was found between AIZ activity and locomotion speed (Figure 3J), providing further support for a specific role for AIZ in regulating direction-switch. Unlike AIY, AIZ did not display much activity beyond reversals (Figure 3H), suggesting that AIZ probably received inhibitory inputs and thereby remained at a rather inactive or low activity state during most time periods (also see below). This imaging data, together with those from laser ablation and optogenetics, strongly suggests that AIZ regulates direction-switch.

The above results suggest a model in which AIY controls direction-switch by forming a circuit with the downstream interneuron AIZ. The fact that AIY suppresses direction-switch but AIZ promotes it suggests that AIY may regulate this behavioral output by inhibiting AIZ. In this case, the nature of the circuit formed by AIY and AIZ would be inhibitory. If so, inhibition of AIY should suppress AIY's inhibitory output to AIZ, which would result in stimulation of AIZ, leading to reversal initiation. To test this model, we recorded the activity of AIZ in response to optogenetic inhibition of AIY in freely behaving worms using the CARIBN system. NpHR inhibition of AIY activated AIZ (Figures 3K and 3L), indicating that AIY inhibited AIZ and disinhibition of AIY promoted reversals. This also supports the prediction that the synaptic connection formed between AIY and AIZ is inhibitory. Interestingly, ChR2 stimulation of AIY did not elicit a notable effect on AIZ activity (Figures 3M and 3N), revealing a nonlinearity of the AIY-AIZ synapse (also see below). Together, our results support the model that AIY regulates direction-switch by forming an inhibitory circuit with the downstream interneuron AIZ (Figure 3O).

AIY Promotes Locomotion Speed by Forming an Excitatory Circuit with RIB

We next sought to identify the neurons that act downstream of AIY to regulate locomotion speed. Laser ablation of RIB, but not AIZ or RIA, abolished the ability of AIY (ChR2) to promote locomotion speed (Figures 4A and 4B), indicating that RIB is required for AIY to regulate locomotion speed. As was the

Figure 3. AIY Regulates Direction-Switch by Forming an Inhibitory Circuit with Its Downstream Neuron AIZ

(A) Schematic showing the major downstream synaptic partners of AIY.

(B) Laser ablation shows that AIZ is required for AIY to promote reversal initiation. Worms expressing NpHR as a transgene in AIY were tested for reversal initiation triggered by yellow light. n = 5. **p < 0.0001 (ANOVA with Tukey's HSD test).

(C) Double ablation of AIZ and AIY suppresses the effect of AIY single ablation on promoting reversal initiation. n ≥ 5. **p < 0.0001 (ANOVA with Tukey's HSD test).

(D and E) Optogenetic inhibition of AIZ activity promotes reversal initiation (D), while optogenetic stimulation of AIZ suppresses it (E). ChR2 and NpHR was expressed as a transgene specifically in AIZ. Control: nontransgenic siblings. n = 5. **p < 0.0001 (t test)

(F and G) Optogenetic inhibition of AIZ does not affect locomotion speed. Because optogenetic stimulation of AIZ triggered reversal initiation, we were unable to test its effect on locomotion speed. (F) Speed traces. (G) Bar graph. n ≥ 18.

(H) Calcium and locomotion velocity traces acquired with the CARIBN system. The windows highlighted in green denote reversals.

(I) Cross-correlogram showing that reversal initiation correlates with AIZ activity increase. n = 5.

(J) Cross-correlation analysis shows that AIZ calcium activity does not show a strong correlation with locomotion speed. n = 5.

(K and L) Inhibition of AIY activates AIZ. Worms carrying two transgenes (one expressing NpHR in AIY and the other expressing GCaMP3.0 in AIZ) were imaged with the CARIBN system. Control: worms carrying the AIZ::GCaMP3.0 transgene only. (K) AIZ GCaMP calcium traces. (l) Bar graph. n ≥ 6. **p < 0.0001 (t test).

(M and N) Stimulation of AIY does not affect the activity of AIZ. Worms carrying two transgenes (one expressing ChR2 in AIY and the other expressing RCaMP in AIZ) were imaged with the CARIBN system. Control: worms carrying the AIZ::RCaMP transgene only. (M) AIZ RCaMP calcium traces. (N) Bar graph. n = 6.

(O) Schematic model showing that AIY forms an inhibitory circuit with AIZ to regulate reversal initiation.

All error bars represent SEM.

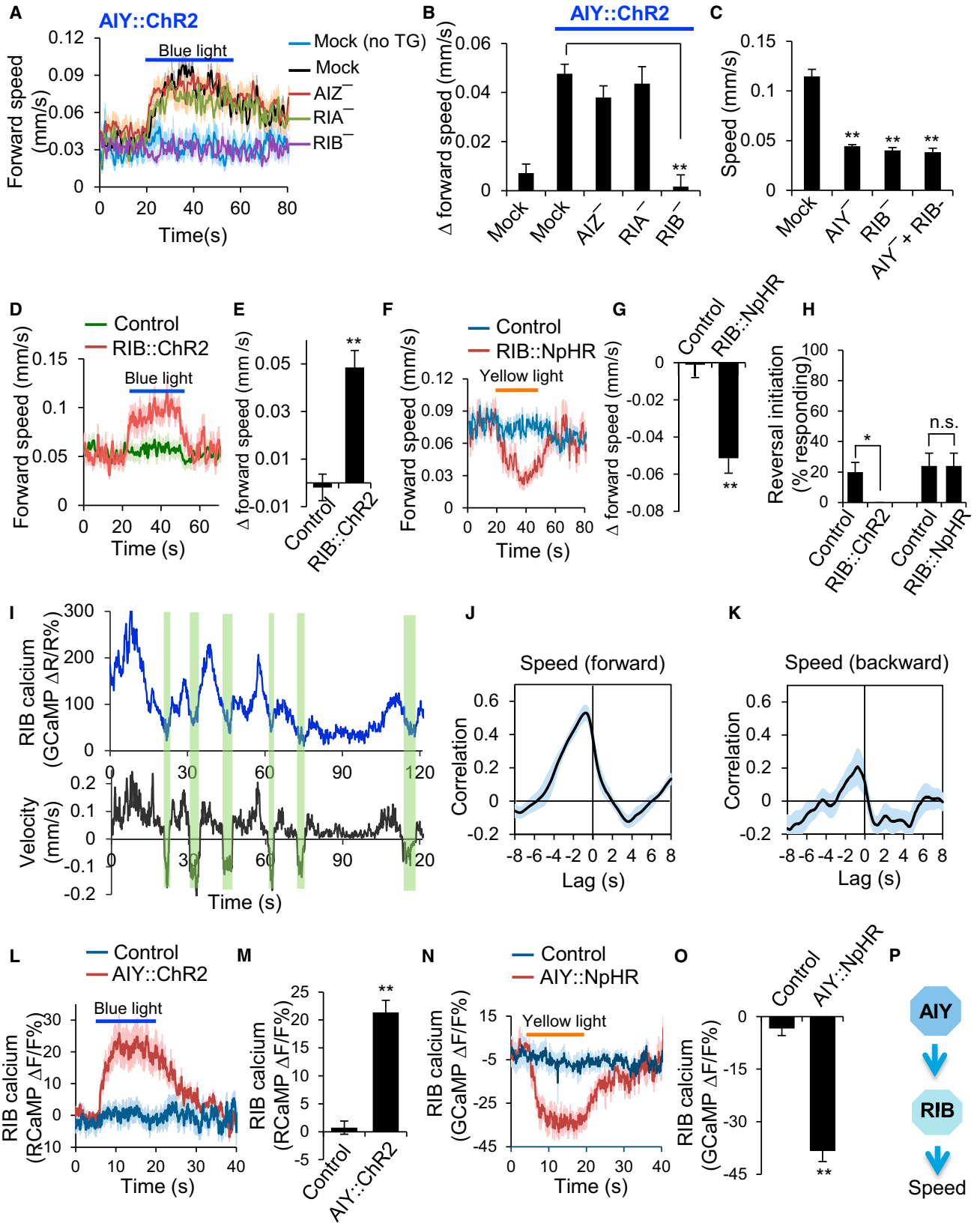

(legend on next page)

case with AIY, ablation of RIB also reduced locomotion speed, and double ablation of AIY and RIB did not exhibit an additive effect (Figure 4C), consistent with the notion that AIY and RIB act in the same pathway to modulate locomotion speed. Notably, laser ablation of RIB does not have a major effect on reversal frequency (Gray et al., 2005). These results suggest that RIB regulates locomotion speed by acting downstream of AIY.

The observation that ablation of RIB reduced locomotion speed suggests that RIB acts to promote locomotion speed. To further test this, we optogenetically interrogated the role of RIB in locomotion speed by expressing ChR2 and NpHR as a transgene specifically in this neuron. ChR2 stimulation of RIB increased locomotion speed (Figures 4D and 4E), while NpHR inhibition of RIB reduced it (Figures 4F and 4G), providing additional evidence that RIB promotes locomotion speed. By contrast, neither NpHR inhibition nor ChR2 stimulation of RIB triggered reversals (Figure 4H), suggesting a specific role for RIB in modulating locomotion speed. Thus, both laser ablation and optogenetic data suggest that RIB promotes locomotion speed.

To provide further evidence, we imaged the activity of RIB in freely behaving worms using the CARIBN system. RIB activity paralleled locomotion speed (Figure 4I). Cross-correlation analysis revealed a strong correlation between RIB activity and forward locomotion speed (but not backward speed) (Figures 4J and 4K). Thus, data from calcium imaging, laser ablation and optogenetics all support a role for RIB in promoting locomotion speed.

The above results point to a model that AIY regulates locomotion speed by forming a circuit with the downstream interneuron RIB. The fact that both AIY and RIB promote locomotion speed suggest that the AIY-RIB circuit is likely excitatory and that AIY may promote locomotion speed by stimulating RIB. To test this model, we recorded the activity of RIB in response to optogenetic stimulation or inhibition of AIY in freely behaving worms using the CARIBN system. ChR2 stimulation of AIY promoted RIB activity (Figures 4L and 4M), while NpHR inhibition of AIY suppressed it (Figures 4N and 4O). Thus, AIY promotes locomotion speed by forming an excitatory circuit with RIB (Figure 4P).

Taken together, our data suggest a model in which AIY regulates direction-switch and locomotion speed by forming two separate downstream circuits: the AIY-AIZ circuit is inhibitory and regulates direction-switch, while the AIY-RIB circuit is excitatory and modulates locomotion speed (Figure 5K).

Both Circuits Employ ACh as a Key Neurotransmitter

Having identified a circuit mechanism by which AIY encodes two distinct behavioral outputs, we then set out to characterize the underlying synaptic mechanisms. We first explored the presynaptic side, asking what neurotransmitter in AIY is critical for controlling direction-switch and locomotion speed. AIY is a cholinergic neuron (Alfonso et al., 1993). We thus examined whether and how blockade of ACh release from AIY would affect these two behavioral outputs. *cha-1* encodes the sole *C. elegans* choline acetyltransferase essential for ACh synthesis (Alfonso et al., 1993). As *cha-1* is expressed in dozens of neurons and *cha-1* mutant worms are severely paralyzed, we were unable to directly assay locomotion behavior in mutant worms. We thus took an RNAi approach by introducing a transgene expressing *cha-1* RNAi specifically in AIY (Figures S3C and S3D). RNAi of *cha-1* in AIY blunted the ability of AIY inhibition (by NpHR) to trigger reversals (Figure 5A) and also suppressed the effect of AIY stimulation (by ChR2) on promoting locomotion speed (Figures 5B and 5C). Furthermore, RNAi of *cha-1* in AIY increased reversal frequency and also reduced locomotion speed (Figures S3A and S3B), an effect similar to that observed in AIY-ablated worms (Figures 1B and 1C). Thus, *cha-1* appears to be required in AIY to control direction-switch and locomotion speed, supporting ACh as a key neurotransmitter in AIY for regulating these two behavioral outputs.

To provide further evidence, we recorded AIY-evoked postsynaptic responses in AIZ and RIB by calcium imaging using the CARIBN system. RNAi of *cha-1* in AIY greatly diminished the postsynaptic calcium response in RIB triggered by AIY (AIY::ChR2) (Figures 5F and 5G). A similar result was obtained with the postsynaptic calcium response in AIZ evoked by AIY (AIY::NpHR) (Figures 5I and 5J). Thus, both behavioral and

Figure 4. AIY Regulates Locomotion Speed by Forming an Excitatory Circuit with Its Downstream Neuron RIB

(A and B) Laser ablation shows that RIB is required for AIY to promote locomotion speed. Worms expressing ChR2 as a transgene in AIY were assayed for locomotion speed in response to blue light. (A) Speed traces. no TG: nontransgenic siblings. (B) Bar graph. $n \geq 16$. $^{**}p < 0.0001$ (ANOVA with Tukey's HSD test).

(C) Double and single ablations of AIY and RIB yield a similar phenotype in locomotion speed. $n \geq 6$. $^{**}p < 0.0001$ (ANOVA with Tukey's HSD test).

(D and E) Optogenetic stimulation of RIB promotes locomotion speed. ChR2 was expressed as a transgene specifically in RIB. Control: nontransgenic siblings. (D) Speed traces. (E) Bar graph. $n \geq 12$. $^{**}p < 0.0001$ (t test).

(F and G) Optogenetic inhibition of RIB suppresses locomotion speed. NpHR was expressed as a transgene specifically in RIB. (F) Speed traces. (G) Bar graph. $n \geq 22$. $^{**}p < 0.0001$ (t test).

(H) Optogenetic manipulation of RIB activity does not trigger reversals. Neither stimulation of RIB by ChR2 nor inhibition of RIB by NpHR triggered reversals. The value for RIB::ChR2 is zero under this condition. $n = 5$. $^{**}p < 0.02$ (t test).

(I) Calcium and locomotion velocity traces acquired with the CARIBN system. The windows highlighted in green denote reversals.

(J and K) Cross-correlation analysis shows that RIB calcium activity exhibits a strong correlation with forward locomotion speed (J) but not with backward locomotion speed (K). $n = 5$.

(L and M) Stimulation of AIY promotes the activity of RIB. Worms carrying two transgenes (one expressing ChR2 in AIY and the other expressing RCaMP in RIB) were imaged with the CARIBN system. Control: worms carrying the RIB::RCaMP transgene only. (L) RIB RCaMP calcium traces. (M) Bar graph. $n \geq 17$. $^{**}p < 0.0001$ (t test).

(N and O) Inhibition of AIY suppresses the activity of RIB. Worms carrying two transgenes (one expressing NpHR in AIY and the other expressing GCaMP3.0 in RIB) were imaged with the CARIBN system. Control: worms carrying the RIB::GCaMP3.0 transgene only. (N) RIB GCaMP3.0 calcium traces. (O) Bar graph. $n \geq 10$. $^{**}p < 0.0001$ (t test)

(P) Schematic model showing that AIY forms an excitatory circuit with RIB to regulate locomotion speed.

All error bars represent SEM. See also Figure S3.

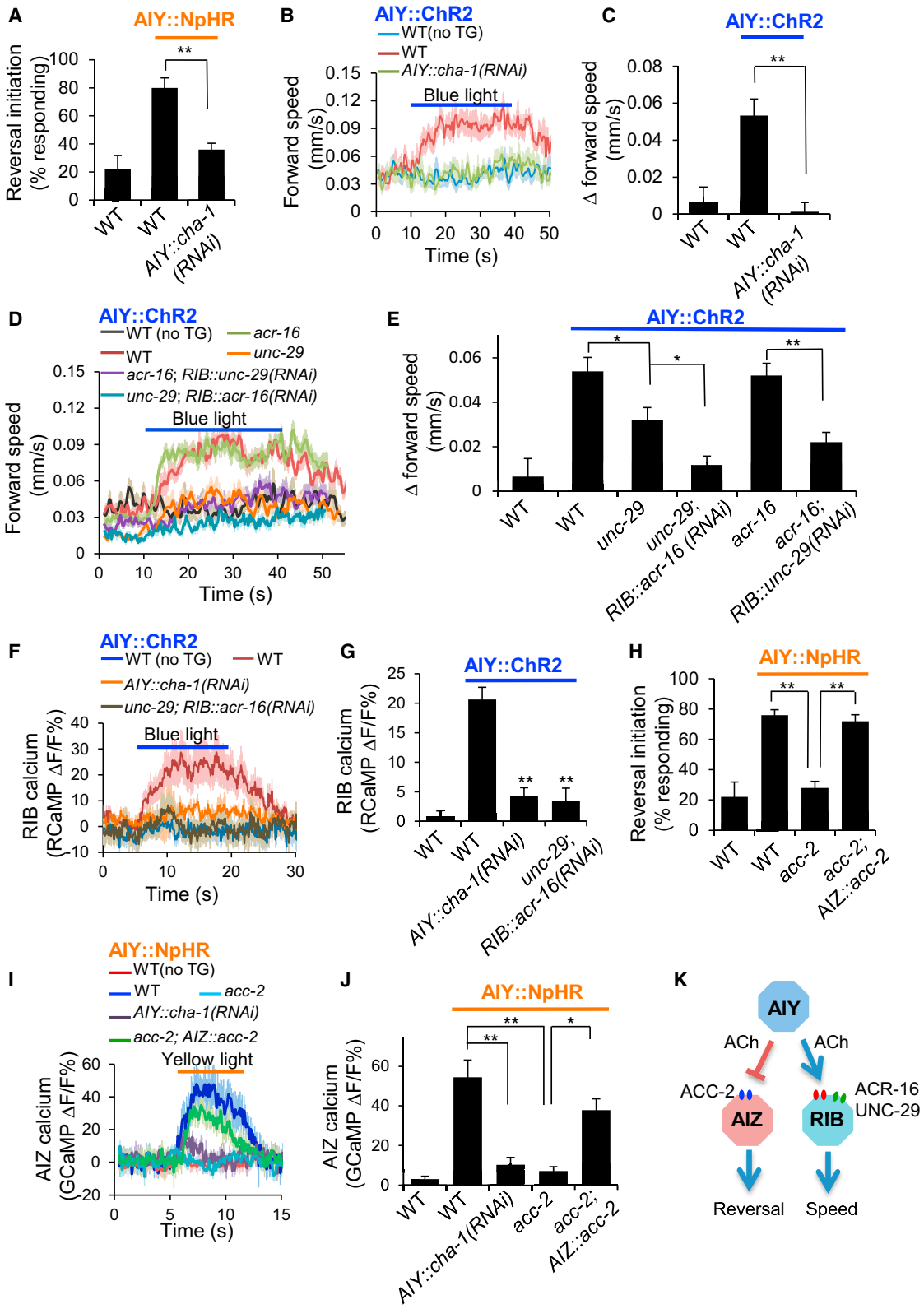

Figure 5. AIY Employs ACh as a Key Neurotransmitter but Recruits Two Distinct Types of Postsynaptic ACh Receptors in AIZ and RIB

(A) RNAi of *cha-1* blunted the ability of AIY to promote reversal initiation. NpHR and *cha-1* RNAi were expressed as separate transgenes specifically in AIY and crossed together. n = 5. **p < 0.0001 (ANOVA with Tukey's HSD test).

(legend continued on next page)

functional imaging data support ACh as a key neurotransmitter in both the AIY-AIZ and AIY-RIB circuits.

The nAChRs UNC-29 and ACR-16 Are Key Components of the Postsynaptic ACh Receptors in RIB

We next sought to identify the postsynaptic ACh receptors expressed in AIZ and RIB. We first searched for candidate receptors in RIB. Our observation that the AIY-RIB synapse is excitatory suggests that the postsynaptic ACh receptor in RIB is probably a cation channel such as nAChR. Two major groups of nAChRs were identified in *C. elegans*: the levamisole-type nAChRs represented by UNC-29 and UNC-38 and the nicotine-type nAChRs such as ACR-16 (Francis et al., 2005; Richmond and Jorgensen, 1999; Touroutine et al., 2005). We decided to examine UNC-29 and ACR-16 because they both are expressed in RIB (Feng et al., 2006; Sherlekar et al., 2013). Loss of UNC-29 modestly but significantly compromised the ability of AIY (AIY::ChR2) to promote locomotion speed, consistent with a role for UNC-29 in regulating locomotion speed (Figures 5D and 5E). This also suggests the presence of additional nAChRs in RIB, which prompted us to test a potential contribution from ACR-16. However, *unc-29; acr-16* double mutant worms are severely paralyzed (Francis et al., 2005), preventing us from directly assaying locomotion behavior in the double mutant. We therefore resorted to the RNAi approach by introducing *acr-16* RNAi as a transgene specifically in RIB in the *unc-29* mutant background and vice versa. *acr-16(RNAi);unc-29* worms showed nearly no increase in locomotion speed in response to ChR2 stimulation of AIY (Figures 5D and 5E). Further, although *acr-16* single mutant worms did not exhibit a notable defect in this behavioral response, *acr-16;unc-29(RNAi)* worms displayed a strong phenotype (Figures 5D and 5E). Thus, UNC-29 and ACR-16 appear to function redundantly. To obtain additional evidence, we recorded AIY-evoked postsynaptic response in RIB by calcium imaging using the CARIBN system. While ChR2 stimulation of AIY elicited a robust postsynaptic response in RIB in wild-type worms, such a response was greatly diminished in worms deficient in both *acr-16* and *unc-29* (Figures 5F and 5G). Thus, both behavioral and functional imaging data suggest ACR-16 and UNC-29 as key components of the postsynaptic ACh receptors in RIB.

ACC-2, an ACh-Gated Cl^- Channel, Is a Key Component of the Postsynaptic ACh Receptor in AIZ

We then set out to identify the postsynaptic ACh receptor in AIZ. The preceding data suggest that the nature of the AIY-AIZ synapse is inhibitory. Then how might ACh, which is best known as an excitatory neurotransmitter, mediate an inhibitory postsynaptic response? Interestingly, the *C. elegans* genome encodes four ACh-gated Cl^- channels: ACC-1, ACC-2, ACC-3, and ACC-4 (Putrenko et al., 2005). We thus tested mutants lacking these ACC channels. Loss of ACC-2 abrogated the ability of AIY (AIY::NpHR) to trigger reversals (Figure 5H), while mutations in the other three ACC channels did not (Figure S3E), uncovering a critical role of ACC-2 in mediating this behavioral output. In addition, worms lacking *acc-2*, but not other *acc* genes, showed an elevated reversal frequency, consistent with the role of ACC-2 as an inhibitory ACh receptor (Figure S3F). We also found that ACC-2 was expressed in AIZ (Figure S3G), and expression of wild-type *acc-2* gene specifically in AIZ rescued the reversal defect of *acc-2* mutant worms (Figure 5H). Again, we recorded AIY-evoked postsynaptic response in AIZ by calcium imaging using the CARIBN system. Loss of ACC-2 greatly diminished AIZ's calcium response triggered by AIY (AIY::NpHR), and transgenic expression of wild-type *acc-2* gene in AIZ rescued this defect (Figures 5I and 5J). Thus, both behavioral and functional imaging data identify ACC-2 as a key component of the postsynaptic ACh receptor in AIZ.

UNC-29/ACR-16 and ACC-2 Are Required for ACh-Gated Cation and Cl^- Current in RIB and AIZ, Respectively

To provide further evidence, we directly recorded ACh-evoked electric responses in AIZ and RIB neurons in dissected animals by whole-cell patch-clamping. ACh elicited an inward current in RIB (Figure 6A). This ACh-gated current exhibited a nearly linear I-V relationship with a positive reversal potential (Figure 6B), consistent with the view that it was mediated by a cation channel. As was the case with our calcium imaging data, mutations in *unc-29* and *acr-16* nearly abolished the ACh-gated current in RIB (Figures 6C and 6D), providing further evidence supporting UNC-29 and ACR-16 as key postsynaptic ACh receptors that mediate the excitatory response in RIB.

By contrast, ACh elicited a different type of current in AIZ (Figures 6E and 6F). This ACh-gated current was outward when clamped at 0 mV with a negative reversal potential, close to the equilibrium potential of Cl^- (Figures 6E and 6F). In addition, increasing the Cl^- concentration in the pipette solution shifted the reversal potential close to 0 mV (Figure 6F), indicating that the current was primarily carried out by a Cl^- channel. Furthermore, mutation in the Cl^- channel ACC-2 nearly eliminated the ACh-gated Cl^- current in AIZ (Figures 6G and 6H). These

(B and C) RNAi of *cha-1* in AIY blunted the ability of AIY to promote locomotion speed. ChR2 and *cha-1* RNAi were expressed as separate transgenes specifically in AIY and crossed together. no TG: nontransgenic siblings. $n \geq 11$. $^{**}p < 0.0006$ (ANOVA with Tukey's HSD test).

(D and E) *unc-29* and *acr-16* act redundantly to promote locomotion speed in RIB. *acr-16* RNAi was introduced as a transgene specifically in RIB. $n \geq 12$. $^{*}p < 0.02$; $^{**}p < 0.0001$ (ANOVA with Tukey's HSD test).

(F and G) Calcium imaging shows that *cha-1*, *unc-29* and *acr-16* mediate the synaptic transmission between AIY and RIB. All worms carried two transgenes with one expressing ChR2 in AIY and the other expressing RCaMP in RIB. (F) RIB RCaMP calcium traces. (G) Bar graph. $n \geq 11$. $^{**}p < 0.0001$ (ANOVA with Tukey's HSD test).

(H) *acc-2* acts in AIZ to promote reversal initiation. $n = 5$. $^{**}p < 0.0001$ (ANOVA with Tukey's HSD test).

(I and J) Calcium imaging shows that *cha-1* and *acc-2* mediate the synaptic transmission between AIY and AIZ. All worms carried two transgenes with one expressing NpHR in AIY and the other expressing GCaMP in AIZ. (I) AIZ GCaMP calcium traces. (J) Bar graph. $n \geq 8$. $^{**}p < 0.0006$ (ANOVA with Tukey's HSD test).

(K) Schematic model.

All error bars represent SEM.

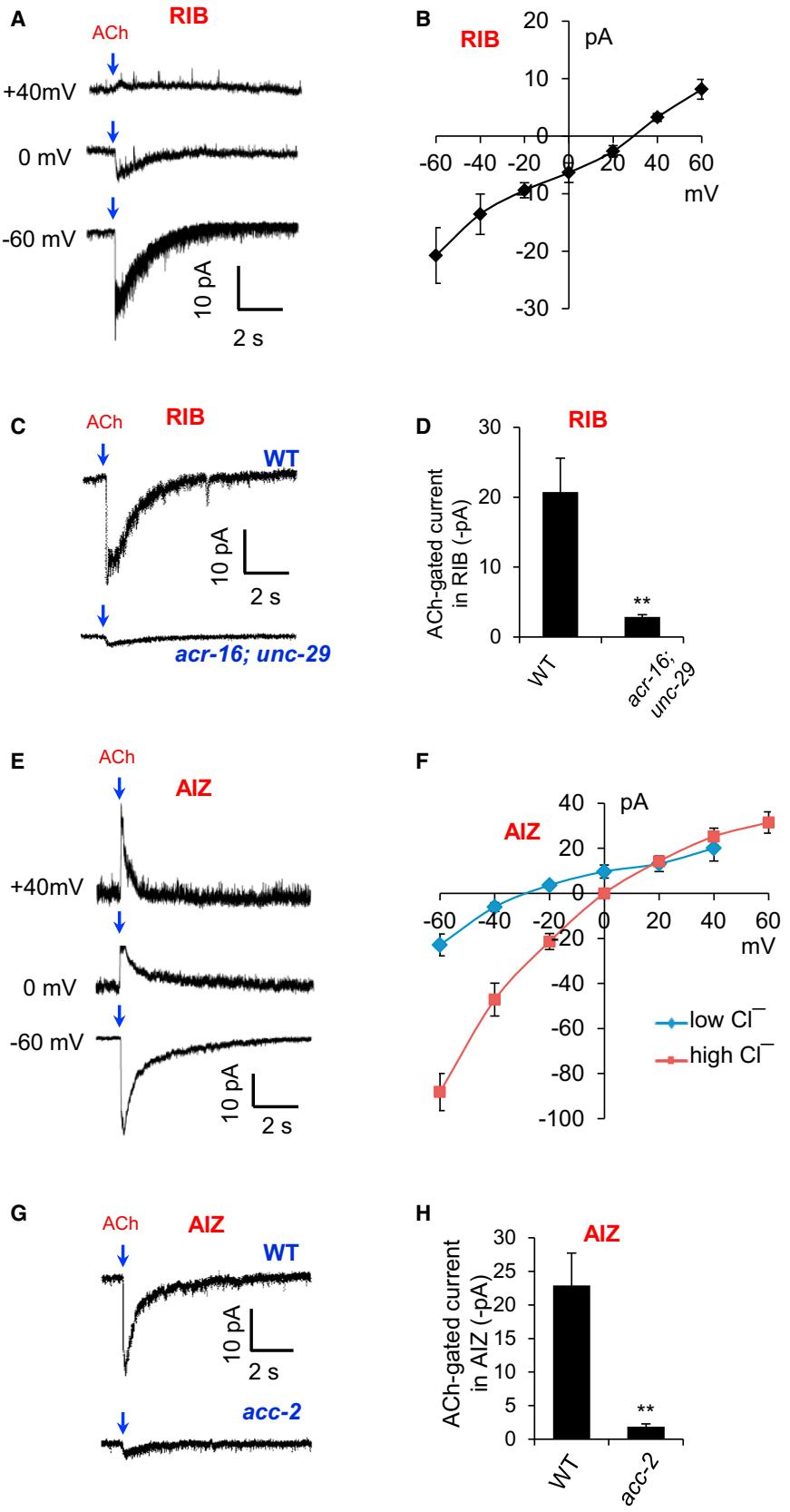

Figure 6. UNC-29/ACR-16 and ACC-2 Are Required for ACh-Gated Cation and Cl^- Current in RIB and AIZ, Respectively

(A and B) Patch-clamp recording shows that ACh evokes a cation current in RIB. (A) Sample traces. (B) I-V relationship. n ≥ 7.

(C and D) ACh-gated current in RIB requires UNC-29 and ACR-16. Voltage: −60 mV. (C) Sample traces. (D) Bar graph. n = 6. **p < 0.002 (t test).

(E and F) Patch-clamp recording shows that ACh evokes a Cl^- current in AIZ. Shown in (E) are sample traces. (F) I-V relationship. Low Cl^-: 25 mM. High Cl^-: 140 mM. n ≥ 5.

(G and H) ACh-gated Cl^- current requires ACC-2. Voltage: −60 mV. (G) Sample traces. (H) Bar graph. n ≥ 6. **p < 0.009 (t test).

All error bars: SEM. ACh: 1 mM.

electrophysiological data further support ACC-2 as a key postsynaptic ACh receptor that mediates the inhibitory response in AIZ.

Differential Processing of AIY Signals by the AIY-RIB and AIY-AIZ Synapses

While the above study identified a circuit and synaptic mechanism by which AIY regulates locomotion speed and direction-switch, it raised one interesting question: In *C. elegans*, although muscle cells fire action potentials (Gao and Zhen, 2011; Liu et al., 2011), most, if not all, neurons are nonspiking and form graded synapses (Goodman et al., 1998; Liu et al., 2009). While this feature may well explain AIY modulation of analog-like behavioral outputs such as locomotion speed, then how is direction-switch, a digital-like behavioral output, regulated by AIY?

As a first step to approach this question, we examined our imaging data collected from freely behaving worms and analyzed the input-output relations between AIY calcium activity (input) and reversal initiation (output) or locomotion speed (output). Both can be fit with a sigmoidal function which is commonly used to describe the input-output relations of neural networks (Mehrotra et al., 1996) (Figures 7A and 7B). Notably, the slope factor of the "reversal" curve, a parameter that describes a curve's steepness, was much smaller than that of the "speed" curve (0.02 versus 0.11). This indicates that reversal probability displayed a much steeper relationship with AIY activity than did locomotion speed (Figures 7A and 7B). In other words, the dynamic range in the "reversal" curve is rather narrow (Figure 7A), as if reversals occurred abruptly as a function of AIY activity, which is consistent with the nature of reversal initiation as an all-or-none digital-like behavioral output. By contrast, the "speed" curve exhibited a much wider dynamic range with locomotion speed changing rather gradually with AIY activity (Figure 7B), a feature that fits well with the nature of locomotion speed as an analog-like behavioral output. In addition, the lower the AIY activity, the higher the reversal probability, but the lower the locomotion speed (Figures 7A and 7B). Thus, AIY activity appears to inversely correlate with reversal probability but positively with locomotion speed. This analysis provides further evidence that AIY activity can differentially encode both analog- and digital-like behavioral outputs.

We then asked how AIY activity might encode both analog- and digital-like behavioral outputs. Because AIY regulates locomotion speed and direction-switch through RIB and AIZ, respectively, we examined the input-output relations of the AIY-RIB and AIY-AIZ synapses. To do so, we optogenetically tuned the activity of AIY (Figure 7C) and then recorded the postsynaptic response in RIB and AIZ by calcium imaging using the CARIBN system in freely behaving animals (Figures 7D and 7E). Based on these data (Figures 7C–7E), we plotted the input-output relations of the two synapses (Figures 7F and 7G). The slope factor of the AIY-AIZ curve was much smaller than that of the AIY-RIB curve (0.04 versus 0.20), indicating that the former possessed a much narrower dynamic range than did the latter (Figures 7F and 7G). In addition, as the $X_{1/2}$ value of the AIY-AIZ curve was smaller than that of the AIY-RIB curve (0.25 versus 0.69), the AIY-AIZ curve was shifted more to the left than the AIY-RIB curve (Figures 7F and 7G). Consequently, AIZ only displayed activity in response to a small window of AIY inputs, but exhibited relatively little or no activity across a large range of AIY inputs (Figure 7F). This is consistent with our preceding calcium imaging data that AIZ showed relatively low activity beyond reversal periods (Figure 3H). As the AIY-AIZ synapse is inhibitory, this analysis suggests that AIZ may be tonically inhibited and locked at an inactive or low activity state over a wide range of inputs from AIY. With a narrow dynamic range, AIZ would then transition from an inactive state to an active state in a very small window, as if it fired in an all-or-none manner with a threshold. This nonlinear transformation strategy would enable the AIY-AIZ synapse to convert graded signals from AIY into a digital-like output in AIZ.

The Postsynaptic ACh Receptors in AIZ and RIB Exhibit Distinct Dynamic Ranges and Ligand Sensitivities

Lastly, we asked what molecular mechanisms may underlie the nonlinear transformation at the AIY-AIZ synapse. In light of the nature of worm synapses, presynaptic ACh release from AIY is likely to be graded. Indeed, optogenetic tuning of AIY activity resulted in graded calcium responses in AIY (Figure 7C). This suggests that the nonlinear transformation may primarily occur at the postsynaptic site. Because of this and the fact that it has not been technically feasible to optically or electrically monitor presynaptic ACh release, we focused on the postsynaptic neurons AIZ and RIB and recorded their electric responses to varying concentrations of ACh in dissected animals by whole-cell patch-clamping (Figures 7H and 7I). In this case, as ACh acted as a ligand to gate ion channels, we fit the data with a Hill equation (Figure 7I). Notably, the Hill slope (Hill coefficient) of the AIZ curve was much greater than that of the RIB curve (4.0 versus 0.66), indicating that the ACh-gated Cl^- channel ACC-2 in AIZ operated over a much narrower dynamic range than did the ACh-gated cation channels ACR-16 and UNC-29 in RIB. Furthermore, the channel in AIZ showed a much higher sensitivity to ACh than did the RIB channel (EC_{50}: 11 μM versus 131 μM) (Figure 7I). Consequently, the AIZ curve is not only steep with a narrow dynamic range, but also shifted more to the left because of its low EC_{50} value (Figure 7I). Given that ACh suppresses AIZ activity, this low EC_{50} value suggests that AIZ would be tonically inhibited and locked at an inactive or low activity state over a wide range of ACh inputs from AIY. The narrow dynamic range would then render AIZ to transition from an inactive or low activity state to an active state within a very small window, as if the neuron fired in an all-or-none fashion with a threshold (Figures 3H and 7F). Thus, the features of the AIY-AIZ and AIY-RIB synapses can be explained at least in part by the distinct biophysical properties of ACh-gated channels expressed in AIZ and RIB. These results uncover a molecular mechanism underlying the nonlinear transformation of AIY signals by the AIY-AIZ synapse. Thus, even if presynaptic release might be graded at a synapse in *C. elegans*, the postsynaptic neuron may adopt a mechanism to transform analog signals into a digital-like output.

DISCUSSION

Due to the immense complexity of the human brain, simple model organisms with a small nervous system are widely used to study how the brain and genes produce behavior (de Bono

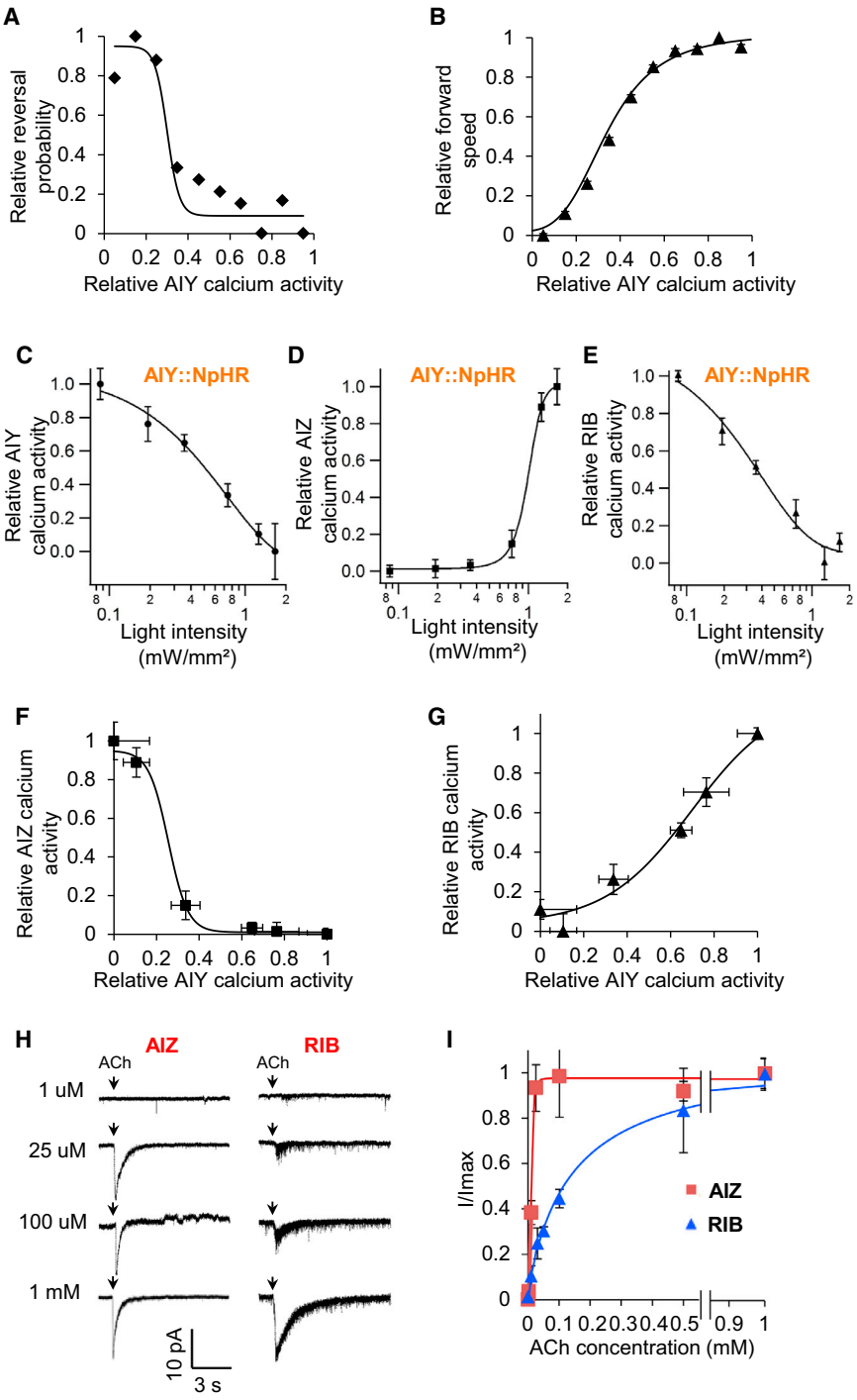

Figure 7. Differential Processing of AIY Signals by the AIY-AIZ and AIY-RIB Synapses

(A and B) The input-output relations between AIY activity (input) and reversal initiation (output) or locomotion speed (output). We analyzed the data from AIY calcium imaging and behavioral traces obtained with the CARIBN system (Figure 2A). AIY calcium data points were extracted from the CARIBN traces, normalized, and binned into ten groups (bin width: 0.1). Reversal probability and locomotion speed was tabulated for each group based on the data from the behavioral traces, normalized, and plotted as a function of the relative AIY calcium activity of individual groups to make (A) and (B), respectively. Both data were fit with a sigmoidal equation: $Y_{output} = 1/(1 + \exp((X_{1/2} - X_{input})/slope))$. $X_{1/2}$ represents the X value where Y shows 50% of its maximal value. *slope* describes the steepness of the curve.

(C–E) Calcium responses in AIY, AIZ, and RIB triggered by optogenetic tuning of AIY activity. Freely behaving worms carrying separate transgenes, which expressed NpHR in AIY (i.e., AIY::NpHR) and GCaMP3 in AIY, AIZ, and RIB, were challenged with varying intensities of yellow light to tune the activity of AIY. Both the presynaptic calcium activity in AIY and the postsynaptic calcium responses in AIZ and RIB were recorded with the CARIBN system. The resulting calcium activities in AIY, AIZ, and RIB were normalized and plotted as a function of yellow light intensities. (C) AIY calcium response curve. (D) AIZ calcium response curve. (E) RIB calcium response curve. $n \geq 4$.

(F and G) The input-output relations of the AIY-AIZ and AIY-RIB synapses. Data in (C–E) were replotted to derive the input-output relations of the two synapses. Specifically, the relative AIZ and RIB calcium activity values (output) shown in (D) and (E) were replotted as a function of the relative AIY calcium activity values (input), which were shown in (C), to generate (F) and (G), respectively. Both data were fit with a sigmoidal equation: $Y_{output} = 1/(1 + \exp((X_{1/2} - X_{input})/slope))$.

(H and I) The postsynaptic ACh receptors in AIZ and RIB show distinct biophysical properties. (H) Sample traces of AIZ and RIB whole-cell currents evoked by different concentrations of ACh. Voltage: −60 mV. (I) ACh-gated currents in AIZ and RIB were plotted as a function of ACh concentrations. Data were fit with a Hill equation: $I/I_{max} = 1/[1 + (EC_{50}/[ACh])^n]$, where n represents Hill slope (Hill coefficient).

All error bars represent SEM.

and Maricq, 2005). The seeming mismatch between the small size of their nervous systems and the large pool of complex behaviors which they execute fuels the suggestion that some of their neurons are probably multifunctional and may regulate multiple behavioral outputs. However, how this is achieved at the circuit and synaptic levels remains largely enigmatic. This is also an important question for mammals, as many neurons in the mammalian brain possess multifunctional properties and can encode multiple outputs (Jankowska, 2001; Schiller, 1996).

In the current report, using a multifaceted approach we have attempted to investigate this question in *C. elegans* by characterizing a model neuron AIY that regulates at least two distinct motor outputs: locomotion speed and direction-switch. Our results show that AIY recruits two distinct downstream

circuits: one (AIY-AIZ) is inhibitory, which regulates direction-switch, while the other one (AIY-RIB) is excitatory, which modulates locomotion speed (Figure 5K). Apparently, at the circuit level, one strategy for a neuron to regulate multiple behavioral outputs is to recruit multiple downstream circuits with each regulating a specific behavioral output. The circuit motifs identified here are highly represented in the nervous system of *C. elegans* and other organisms including mammals (Sporns and Kötter, 2004), raising the possibility that this might be a common strategy adopted by neurons in worms and perhaps other organisms to regulate multiple behavioral outputs.

Nevertheless, it should be noted that neural control of behavior is rather complex. For example, the two circuits identified here must involve additional neurons. Indeed, we found that the neurons acting downstream of AIZ in the circuit are backward command interneurons and RIM known to control reversal initiation, while RIB acts through AVB, a forward command interneuron that promotes forward locomotion speed (Z.L. and X.Z.S.X., unpublished data) (Chalfie et al., 1985; Piggott et al., 2011). Additionally, as these two circuits have connections with other neurons, they probably do not function in isolation and may engage in crosstalk with other circuits and may be modulated by inputs from other interneurons and sensory neurons. Further, the two circuits may also crosstalk with each other. For example, the fact that AIY inhibition triggers reversals in RIB-ablated worms suggests that AIZ may signal to other neurons in the speed circuit. Lastly, other circuit mechanisms must be employed by worms to encode multiple behavioral outputs.

By characterizing the underlying synaptic mechanisms, we show that both the AIY-AIZ and AIY-RIB circuits employ ACh as a key neurotransmitter in AIY but utilize two distinct types of postsynaptic ACh receptors in AIZ and RIB, with one in AIZ being an inhibitory ACh-gated Cl^- channel and the other in RIB being excitatory nAChRs (Figure 5K). With this synaptic mechanism, AIY is able to signal downstream neurons both positively and negatively with a single neurotransmitter, thereby enriching its capacity to encode multiple behavioral outputs. Apparently, AIY is a highly versatile interneuron and regulates additional behavioral outputs such as head bending and turns in chemotaxis and thermotaxis (Chalasani et al., 2007; Ha et al., 2010; Kocabas et al., 2012; Mori and Ohshima, 1995). AIY is certainly not the only such neuron in *C. elegans*, and other neurons may also regulate multiple behavioral outputs (Bargmann, 2012; de Bono and Maricq, 2005). The multidisciplinary approach utilized in the current study, which integrates calcium imaging, optogenetics, molecular genetics, laser ablation, and electrophysiology, shall be instrumental in elucidating the circuit, synaptic, and molecular mechanisms by which worm neurons encode multiple behavioral outputs at the single neuron resolution.

One interesting feature of *C. elegans* neurons is that they are nonspiking and release neurotransmitters in a graded manner. This is also the case for many neurons in mammals and insects, for example, photoreceptor neurons and bipolar cells in the retina, as well as cochlear hair cells in the inner ear (Bargmann and Marder, 2013). Graded synaptic release is also observed at dendrodendritic synapses in both vertebrates and invertebrates (Shepherd et al., 2007). While it is easy to appreciate the encoding of analog-like outputs by graded synapses, the question arises as to how these synapses could also encode digital-like outputs. This appears to be a long-standing question in *C. elegans*, as worms clearly execute many types of digital-like behavioral outputs (e.g., reversal initiation, omega turn, egg-laying, defecation, etc.). By characterizing the AIY-AIZ synapse, we have now demonstrated in *C. elegans* that the biophysical properties of ion channels in postsynaptic neurons can help transform graded presynaptic inputs into a digital-like postsynaptic output, providing a molecular explanation. Apparently, the synapses in *C. elegans* are quite versatile. The biophysical properties of the channel in AIZ are not unique and are also found in other types of neurotransmitter-gated ion channels in both vertebrates and invertebrates. For example, certain types of $GABA_A$ receptors, 5-HT3 receptors, nAChRs, and histamine-gated Cl^- channels also show high sensitivity with a narrow dynamic range (high Hill coefficient) (Chang et al., 2001; McLaughlin et al., 2009; Rammes et al., 2009). As such, the mechanism identified here might represent a common strategy that contributes to the nonlinear transformation of synaptic signals at graded synapses and perhaps some binary synapses as well.

EXPERIMENTAL PROCEDURES

Calcium Imaging, Optogenetics, and Behavioral Assays

Calcium imaging was performed on freely behaving worms using the CARIBN system as previously described (Piggott et al., 2011). Day 1 adult worms were used for imaging under the standard laboratory condition on nematode growth media (NGM) plates covered with a thin layer of OP50 bacteria (20°C, 30% humidity). All imaging experiments were performed on *lite-1(xu7)* worms that do not show phototaxis response (Liu et al., 2010). Traces were passed through a binomial low-pass filter. We imaged calcium transients in RIB soma. In AIY and AIZ, we imaged their processes as they show most robust calcium signals (Chalasani et al., 2007). In many cases, ratiometric imaging was conducted on worms coexpressing GCaMP3 and DsRed. In these cases, $\Delta R/R$ was used to quantify fluorescence changes. As single wavelength fluorescence imaging also works well under our system, this protocol was used in some cases, particularly those using RCaMP (Akerboom et al., 2013), as well as experiments involving simultaneous calcium imaging and optogenetic interrogation. In these cases, $\Delta F/F$ was used to quantify fluorescence changes.

To combine calcium imaging and optogenetic interrogation, a separate LED light source emitting yellow light and blue light was added to the CARIBN system to turn on NpHR and ChR2, respectively.

Optogenetic interrogation of reversal initiation was performed as previously described (Piggott et al., 2011). Briefly, worms were grown on NGM plates supplied with 5 μM all-trans retinal and tested on retinal-free NGM plates spread with a thin layer of OP50 bacteria. Blue light (5 s pulse; 470 ± 20 nm; ~0.5 mW/mm^2) and yellow light (5 s pulse; 575 ± 25 nm; 2 mW/mm^2) was delivered from an Arc lamp (EXFO) by a 10× objective (Zeiss M2Bio) to the head of a forward-moving worm to activate ChR2 and NpHR to trigger reversals, respectively. We scored it as a positive response if the animal stopped forward movement and also initiated a reversal lasting at least half of a head swing. Each worm was tested five times.

Spontaneous locomotion behavior was analyzed using an automated worm tracking system as described previously (Feng et al., 2006). Worms were tracked for 10 min. Mean speed and reversal events were tabulated over the entire 10 min window.

To optogenetically interrogate locomotion speed, on the tracking system we placed a separate LED light source emitting yellow light and blue light to turn on NpHR and ChR2, respectively. In general, a 30 s of light pulse was delivered. Mean speed (forward speed) was therefore calculated over a 30 s window. The very few reversal events were removed from these speed traces for clarity, and no gaps remained in the averaged trace because they were

averaged out between different animals. Laser ablation was conducted using standard protocols.

Electrophysiology

Patch-clamp recordings were conducted on an Olympus upright microscope with an EPC-10 amplifier, a micromanipulator, and PatchMaster software as previously described (Li et al., 2011; Ward et al., 2008). Briefly, worms were glued and dissected on a sylgard-coated coverglass. Normal bath solution (in mM): 145 NaCl, 5 KCl, 1 $CaCl_2$, 5 $MgCl_2$, 11 dextrose, and 10 HEPES (330 mOsm; pH adjusted to 7.3). Normal pipette solution: 115 K-gluconate, 15 KCl, 5 $MgCl_2$, 10 HEPES, 0.25 $CaCl_2$, 20 sucrose, 5 EGTA, 5 Na_2ATP, and 0.5 NaGTP. KCl (115 mM) was used to replace K-gluconate to make high Cl^- pipette solution. ACh was diluted in bath solution and perfused toward the neuron of interest which was marked by a YFP or mCherry transgene. Series resistance and membrane capacitance were both compensated during recording.

SUPPLEMENTAL INFORMATION

Supplemental Information includes Extended Experimental Procedures, three figures, and one movie and can be found with this article online at http://dx.doi.org/10.1016/j.cell.2014.09.056.

ACKNOWLEDGMENTS

We thank Bing Ye for technical assistance and helpful discussions, and Liz Ronan and Bing Ye for critically reading the manuscript. Some strains were obtained from the Caenorhabditis Genetics Center (CGC) and Knockout Consortiums in the United States and Japan. This work was supported by grants from the NIH (X.Z.S.X.).

Received: June 10, 2014
Revised: August 12, 2014
Accepted: September 24, 2014
Published: November 6, 2014

REFERENCES

Akerboom, J., Carreras Calderón, N., Tian, L., Wabnig, S., Prigge, M., Tolö, J., Gordus, A., Orger, M.B., Severi, K.E., Macklin, J.J., et al. (2013). Genetically encoded calcium indicators for multi-color neural activity imaging and combination with optogenetics. Front. Mol. Neurosci. *6*, 2.

Alfonso, A., Grundahl, K., Duerr, J.S., Han, H.P., and Rand, J.B. (1993). The Caenorhabditis elegans unc-17 gene: a putative vesicular acetylcholine transporter. Science *261*, 617–619.

Bargmann, C.I. (2012). Beyond the connectome: how neuromodulators shape neural circuits. BioEssays *34*, 458–465.

Bargmann, C.I., and Marder, E. (2013). From the connectome to brain function. Nat. Methods *10*, 483–490.

Berkowitz, A., Roberts, A., and Soffe, S.R. (2010). Roles for multifunctional and specialized spinal interneurons during motor pattern generation in tadpoles, zebrafish larvae, and turtles. Front. Behav. Neurosci. *4*, 36.

Briggman, K.L., and Kristan, W.B. (2008). Multifunctional pattern-generating circuits. Annu. Rev. Neurosci. *31*, 271–294.

Brown, E.N., Kass, R.E., and Mitra, P.P. (2004). Multiple neural spike train data analysis: state-of-the-art and future challenges. Nat. Neurosci. *7*, 456–461.

Chalasani, S.H., Chronis, N., Tsunozaki, M., Gray, J.M., Ramot, D., Goodman, M.B., and Bargmann, C.I. (2007). Dissecting a circuit for olfactory behaviour in Caenorhabditis elegans. Nature *450*, 63–70.

Chalfie, M., Sulston, J.E., White, J.G., Southgate, E., Thomson, J.N., and Brenner, S. (1985). The neural circuit for touch sensitivity in Caenorhabditis elegans. The Journal of neuroscience *5*, 956–964.

Chang, Y., Xie, Y., and Weiss, D.S. (2001). Positive allosteric modulation by ultraviolet irradiation on GABA(A), but not GABA(C), receptors expressed in Xenopus oocytes. J. Physiol. *536*, 471–478.

de Bono, M., and Maricq, A.V. (2005). Neuronal substrates of complex behaviors in C. elegans. Annu. Rev. Neurosci. *28*, 451–501.

de Bono, M., Tobin, D.M., Davis, M.W., Avery, L., and Bargmann, C.I. (2002). Social feeding in Caenorhabditis elegans is induced by neurons that detect aversive stimuli. Nature *419*, 899–903.

Feng, Z., Li, W., Ward, A., Piggott, B.J., Larkspur, E.R., Sternberg, P.W., and Xu, X.Z.S. (2006). A C. elegans model of nicotine-dependent behavior: regulation by TRP-family channels. Cell *127*, 621–633.

Francis, M.M., Evans, S.P., Jensen, M., Madsen, D.M., Mancuso, J., Norman, K.R., and Maricq, A.V. (2005). The Ror receptor tyrosine kinase CAM-1 is required for ACR-16-mediated synaptic transmission at the C. elegans neuromuscular junction. Neuron *46*, 581–594.

Gao, S., and Zhen, M. (2011). Action potentials drive body wall muscle contractions in Caenorhabditis elegans. Proc. Natl. Acad. Sci. USA *108*, 2557–2562.

Goodman, M.B., Hall, D.H., Avery, L., and Lockery, S.R. (1998). Active currents regulate sensitivity and dynamic range in C. elegans neurons. Neuron *20*, 763–772.

Gray, J.M., Hill, J.J., and Bargmann, C.I. (2005). A circuit for navigation in Caenorhabditis elegans. Proc. Natl. Acad. Sci. USA *102*, 3184–3191.

Ha, H.I., Hendricks, M., Shen, Y., Gabel, C.V., Fang-Yen, C., Qin, Y., Colón-Ramos, D., Shen, K., Samuel, A.D., and Zhang, Y. (2010). Functional organization of a neural network for aversive olfactory learning in Caenorhabditis elegans. Neuron *68*, 1173–1186.

Jankowska, E. (2001). Spinal interneuronal systems: identification, multifunctional character and reconfigurations in mammals. J. Physiol. *533*, 31–40.

Kocabas, A., Shen, C.H., Guo, Z.V., and Ramanathan, S. (2012). Controlling interneuron activity in Caenorhabditis elegans to evoke chemotactic behaviour. Nature *490*, 273–277.

Li, W., Kang, L., Piggott, B.J., Feng, Z., and Xu, X.Z.S. (2011). The neural circuits and sensory channels mediating harsh touch sensation in Caenorhabditis elegans. Nat. Commun. *2*, 315.

Liu, K.S., and Sternberg, P.W. (1995). Sensory regulation of male mating behavior in Caenorhabditis elegans. Neuron *14*, 79–89.

Liu, Q., Hollopeter, G., and Jorgensen, E.M. (2009). Graded synaptic transmission at the Caenorhabditis elegans neuromuscular junction. Proc. Natl. Acad. Sci. USA *106*, 10823–10828.

Liu, J., Ward, A., Gao, J., Dong, Y., Nishio, N., Inada, H., Kang, L., Yu, Y., Ma, D., Xu, T., et al. (2010). C. elegans phototransduction requires a G protein-dependent cGMP pathway and a taste receptor homolog. Nat. Neurosci. *13*, 715–722.

Liu, P., Ge, Q., Chen, B., Salkoff, L., Kotlikoff, M.I., and Wang, Z.W. (2011). Genetic dissection of ion currents underlying all-or-none action potentials in C. elegans body-wall muscle cells. J. Physiol. *589*, 101–117.

McLaughlin, J.T., Barron, S.C., See, J.A., and Rosenberg, R.L. (2009). Conformational changes in alpha 7 acetylcholine receptors underlying allosteric modulation by divalent cations. BMC Pharmacol. *9*, 1.

Mehrotra, K., Mohan, C.K., and Ranka, S. (1996). Elements of Artificial Neural Networks (A Bradford Book), (Cambridge, MA: MIT Press).

Mori, I., and Ohshima, Y. (1995). Neural regulation of thermotaxis in Caenorhabditis elegans. Nature *376*, 344–348.

Piggott, B.J., Liu, J., Feng, Z., Wescott, S.A., and Xu, X.Z.S. (2011). The neural circuits and synaptic mechanisms underlying motor initiation in C. elegans. Cell *147*, 922–933.

Putrenko, I., Zakikhani, M., and Dent, J.A. (2005). A family of acetylcholine-gated chloride channel subunits in Caenorhabditis elegans. J. Biol. Chem. *280*, 6392–6398.

Raizen, D.M., Zimmerman, J.E., Maycock, M.H., Ta, U.D., You, Y.J., Sundaram, M.V., and Pack, A.I. (2008). Lethargus is a Caenorhabditis elegans sleep-like state. Nature *451*, 569–572.

Rammes, G., Hosp, C., Eisensamer, B., Tanasic, S., Nothdurfter, C., Zieglgänsberger, W., and Rupprecht, R. (2009). Identification of a domain

which affects kinetics and antagonistic potency of clozapine at 5-HT3 receptors. PLoS ONE *4*, e6715.

Richmond, J.E., and Jorgensen, E.M. (1999). One GABA and two acetylcholine receptors function at the C. elegans neuromuscular junction. Nat. Neurosci. *2*, 791–797.

Schiller, P.H. (1996). On the specificity of neurons and visual areas. Behav. Brain Res. *76*, 21–35.

Shepherd, G.M., Chen, W.R., Willhite, D., Migliore, M., and Greer, C.A. (2007). The olfactory granule cell: from classical enigma to central role in olfactory processing. Brain Res. Brain Res. Rev. *55*, 373–382.

Sherlekar, A.L., Janssen, A., Siehr, M.S., Koo, P.K., Caflisch, L., Boggess, M., and Lints, R. (2013). The C. elegans male exercises directional control during mating through cholinergic regulation of sex-shared command interneurons. PLoS ONE *8*, e60597.

Sokolowski, M.B. (2001). Drosophila: genetics meets behaviour. Nat. Rev. Genet. *2*, 879–890.

Sporns, O., and Kötter, R. (2004). Motifs in brain networks. PLoS Biol. *2*, e369.

Touroutine, D., Fox, R.M., Von Stetina, S.E., Burdina, A., Miller, D.M., 3rd, and Richmond, J.E. (2005). acr-16 encodes an essential subunit of the levamisole-resistant nicotinic receptor at the Caenorhabditis elegans neuromuscular junction. J. Biol. Chem. *280*, 27013–27021.

Tsalik, E.L., and Hobert, O. (2003). Functional mapping of neurons that control locomotory behavior in Caenorhabditis elegans. J. Neurobiol. *56*, 178–197.

Ward, A., Liu, J., Feng, Z., and Xu, X.Z. (2008). Light-sensitive neurons and channels mediate phototaxis in C. elegans. Nat. Neurosci. *11*, 916–922.

Zhang, F., Wang, L.P., Brauner, M., Liewald, J.F., Kay, K., Watzke, N., Wood, P.G., Bamberg, E., Nagel, G., Gottschalk, A., and Deisseroth, K. (2007). Multimodal fast optical interrogation of neural circuitry. Nature *446*, 633–639.

Zheng, Y., Brockie, P.J., Mellem, J.E., Madsen, D.M., and Maricq, A.V. (1999). Neuronal control of locomotion in C. elegans is modified by a dominant mutation in the GLR-1 ionotropic glutamate receptor. Neuron *24*, 347–361.

EXTENDED EXPERIMENTAL PROCEDURES

Strains

WT: N2. TQ800: *lite-1(xu7).* TQ275: *acr-16(ok789).* TQ365: *unc-29(e193).* TQ1252: *xuEx21[Pnpr-9::YFP, Pnpr-9::DsRed, Punc-122::GFP].* TQ3041: *xuEx1042[Pser-2(2)::frt::GFP, Podr-2(2b)::flp, Punc-122::GFP]; lite-1(xu7).* TQ3051: *xuEx1046[Pgcy-28d::sl2::YFP].* TQ3142: *xuEx1084[Pser-2(2)::frt::NpHR, Podr-2(2b)::flp, Punc-122::GFP]; lite-1(xu7).* TQ3296: *xuIs204[Pser-2(2)::frt::NpHR::YFP, Podr-2(2b)::flp,Punc-122::YFP]; lite-1(xu7).* TQ3301: *xuIs198[Pser-2(2)::frt::ChR2::YFP,Podr-2(2b)::flp,Punc-122::YFP]; lite-1(xu7).* TQ3509: *xuIs230[Pttx-3s::NpHR::YFP, Pttx-3s::DsRed, Punc-122::YFP]; lite-1(xu7).* TQ3513: *xuIs230[Pttx-3s::NpHR::YFP, Pttx-3s::DsRed,Punc-122::YFP]; xuEx1044[Podr-2a(3b)::sl2::YFP]; lite-1(xu7).* TQ3516: *xuIs230[Pttx-3s::NpHR::YFP, Pttx-3s::DsRed, Punc-122::YFP]; njIs10[Pglr-3::GFP]; lite-1(xu7).* TQ3538: *xuEx1177[Pttx-3::GCaMP3.0,Pttx-3s::DsRed]; lite-1(xu7).* TQ4138: *xuIs223 [Pttx-3s::ChR2::YFP, Pttx-3s::DsRed, Punc-122::YFP]; xuEx1279[Psto-3s::sl2::YFP]; lite-1(xu7).* TQ4151: *xuIs230[Pttx-3s::NpHR::YFP, Pttx-3s::DsRed, Punc-122::YFP]; xuEx1279[Psto-3l::sl2::YFP]; lite-1(xu7).* TQ4232: *acc-2(ok2216).* TQ4250: *xuEx1396[Psto-3s::ChR2::YFP,lin-15(+)]; lite-1.* TQ4268: *xuEx1398[Psto-3s::NpHR::YFP, lin-15(+)]; lite-1.* TQ4270: *xuEx1394[Psto-3s::GCaMP3.0, Psto-3s::mCherry, lin-15(+)]; lite-1; lin-15 (n765).* TQ4274: *xuIs223[Pttx-3s::ChR2::YFP, Pttx-3s::DsRed, Punc-122::YFP]; lite-1(xu7).* TQ4277: *xuIs223[Pttx-3s::ChR2::YFP, Pttx-3s::DsRed, Punc-122::YFP]; njIs10[Pglr-3::GFP]; lite-1(xu7).* TQ4288: *acc-1(tm3268).* TQ4510: *xuIs230[Pttx-3s::NpHR::YFP, Pttx-3s::DsRed, Punc-122::YFP]; xuEx1414[Pttx-3s::cha-1(RNAi), Psto-3s::cfp, Pttx-3s::cfp]; lite-1.* TQ4511: *xuIs230[Pttx-3s::NpHR::YFP, Pttx-3s::DsRed, Punc-122::YFP]; acc-1(tm3268); lite-1.* TQ4512: *xuIs230[Pttx-3s::NpHR::YFP, Pttx-3s::DsRed, Punc-122::YFP]; acc-2(ok2216); lite-1.* TQ4515: *xuIs230[Pttx-3s::NpHR::YFP, Pttx-3s::DsRed, Punc-122::YFP]; acc-3(ok3450); lite-1.* TQ4517: *xuIs230[Pttx-3s::NpHR::YFP, Pttx-3s::DsRed, Punc-122::YFP]; acc-4(ok2371); lite-1.* TQ4519: *acc-3(ok3450).* TQ4520: *acc-4(ok2371).* TQ4555: *xuIs222[Pttx-3s::ChR2::YFP, Pttx-3s::DsRed, Punc-122::YFP]; xuEx1414 [Pttx-3s::cha-1(RNAi), Psto-3s::cfp, Pttx-3s::cfp]; lite-1.* TQ4692: *unc-29(e293); xuIs222[Pttx-3s::ChR2::YFP, Pttx-3s::DsRed, Punc-122::YFP]; xuEx1512[Psto-3s::RCaMP1h, lin-15(+)]; lite-1.* TQ4849: *xuEx1500[Pacc-2::acc-2(genomic DNA)::sl2::YFP, lin-15(+)]; xuEx1520[Pser-2(2)::frt::mCherry, Podr-2(2b)::flp, Psto-3s::sl2::mCherry, lin-15(+)]; lite-1.* TQ4850: *acr-16(ok789); xuIs222[Pttx-3s::ChR2::YFP, Pttx-3s::DsRed, Punc-122::YFP]; lite-1.* TQ4854: *unc-29(e293); xuIs222[Pttx-3s::ChR2::YFP, Pttx-3s::DsRed, Punc-122::YFP]; lite-1.* TQ4964 *xuIs230[Pttx-3s::nphr::yfp+Pttx-3s::DsRed+Punc-122d::yfp]; acc-2(ok2216); xuEx1534[Podr-2b(3a)::acc-2(genomic DNA)::sl2::mcherry]; lite-1.* TQ4982: *xuIs230[Pttx-3s::NpHR::YFP, Pttx-3s::DsRed, Punc-122::YFP]; xuIs272 [Pser-2(2)::frt::Gcamp3.0, Podr-2(2b)::flp, lin-15(+)]; xuEx1414[Pttx-3s::cha-1(RNAi), Psto-3s::cfp, Pttx-3s::cfp]; lite-1.* TQ4985: *xuIs230[Pttx-3s::NpHR::YFP, Pttx-3s::DsRed, Punc-122::YFP]; xuIs272[Pser-2(2)::frt::Gcamp3.0, Podr-2(2b)::flp, lin-15(+)]; lite-1.* TQ4998: *unc-29(e193); xuIs222[Pttx-3s::ChR2::YFP, Pttx-3s::DsRed, Punc-122::YFP]; xuEx1557[Psto-3s::acr-16(RNAi)]; lite-1.* TQ5023: *xuIs272[Pser-2(2)::frt::Gcamp3.0, Podr-2(2b)::flp,lin-15(+)]; lite-1.* TQ5025: *xuEx1512[Psto-3s::RCaMP1h,lin-15(+)]; xuIs222 [Pttx-3s::ChR2::YFP,Pttx-3s::DsRed,Punc-122::YFP]; xuEx1414[Pttx-3s::cha-1(RNAi), Psto-3s::cfp, Pttx-3s::cfp]; lite-1.* TQ5260: *xuEx1698[Psto-3s::mCherry, Pttx-3s::sl2::YFP]; lite-1.* TQ5262: *xuEx1700[Pttx-3s::DsRed]; xuEx1042[Pser-2(2)::frt::GFP, Podr-2(2b)::flp, Punc-122::GFP]; lite-1(xu7).* TQ5343: *xuEx1042[Pser-2(2)::frt::GFP, Podr-2(2b)::flp, Punc-122::GFP]; xuIs223 [Pttx-3s::ChR2::YFP, Pttx-3s::DsRed, Punc-122::YFP]; lite-1(xu7).* TQ5344: *acc-2(ok2216); xuIs230[Pttx-3s::NpHR::YFP, Pttx-3s::DsRed, Punc-122::YFP]; xuIs272[Pser-2(2)::frt::Gcamp3.0, Podr-2(2b)::flp, lin-15(+)]; lite-1.* TQ5348: *acc-2(ok2216); xuIs230 [Pttx-3s::NpHR::YFP, Pttx-3s::DsRed, Punc-122::YFP]; xuEx1534[Podr-2(2b)(3a)::acc-2(genomic DNA)::sl2::mCherry]; xuIs272 [Pser-2(2)::frt::Gcamp3.0, Podr-2(2b)::flp, lin-15(+)]; lite-1.* TQ5350: *unc-29(e193); xuIs222[Pttx-3s::ChR2::YFP, Pttx-3s::DsRed, Punc-122::YFP]; xuEx1557[Psto-3s::acr-16(RNAi)]; xuEx1512[Psto-3s::RCaMP1h, lin-15(+)]; lite-1.* TQ5352: *xuIs302[Pttx-3s::NpHR::mCherry]; xuIs272[Pser-2(2)::frt::Gcamp3.0, Podr-2(2b)::flp, lin-15(+)]; lite-1.* TQ5452: *xuEx1700[Pttx-3s::DsRed]; lite-1.* TQ5772: *xuIs294[Pttx-3s::ChR2::YFP]; xuIs336[Pser-2(2)::frt::RCaMP1h, Podr-2(2b)::flp, lin-15(+)]; lite-1.* TQ5773: *xuIs330[Psto-3s::RCaMP1h]; xuIs294[Pttx-3s::ChR2::YFP]; lite-1.* TQ5774: *xuIs302[Pttx-3s::NpHR::mCherry]; xuIs324[Psto-3s::GCaMP3.0]; lite-1.* TQ5775: *xuIs302[Pttx-3s::NpHR::mCherry]; xuIs311[Pttx-3::GCaMP3.0]; lite-1*.

Molecular Biology

Promoters labeling specific neurons are described as follows: AIA: *gcy-28d*, AIB: *npr-9*, AIY: *ttx-3 s*, RIB: *sto-3 s*, AIZ: *ser-2(2) + odr-2(2b)* with the FLP/FRT strategy (Bendena et al., 2008; Davis et al., 2008; Kratz, 2010; Schmitt et al., 2012; Shinkai et al., 2011; Tsalik et al., 2003). Neuron-specific RNAi was generated as described previously (Esposito et al., 2007). The *acr-16* RNAi segment was amplified with the primers *5′-cacagatgtccgttttccagctg* and *5′- catgcctgttcttccttatcacc*, and the *cha-1* RNAi segment was amplified with *5′- acaagttcgtgcgtcaagctactc* and *5′-aataaatccatccggactgacac* from N2 genomic DNA.

SUPPLEMENTAL REFERENCES

Bendena, W.G., Boudreau, J.R., Papanicolaou, T., Maltby, M., Tobe, S.S., and Chin-Sang, I.D. (2008). A Caenorhabditis elegans allatostatin/galanin-like receptor NPR-9 inhibits local search behavior in response to feeding cues. Proc. Natl. Acad. Sci. USA *105*, 1339–1342.

Davis, M.W., Morton, J.J., Carroll, D., and Jorgensen, E.M. (2008). Gene activation using FLP recombinase in C. elegans. PLoS Genet. *4*, e1000028.

Esposito, G., Di Schiavi, E., Bergamasco, C., and Bazzicalupo, P. (2007). Efficient and cell specific knock-down of gene function in targeted C. elegans neurons. Gene *395*, 170–176.

Kratz, J.E. (2010). Prohibitin Homology Domain Proteins in Caenorhabditis elegans (New York: Columbia University), p. 193.

Schmitt, C., Schultheis, C., Pokala, N., Husson, S.J., Liewald, J.F., Bargmann, C.I., and Gottschalk, A. (2012). Specific expression of channelrhodopsin-2 in single neurons of Caenorhabditis elegans. PLoS ONE *7*, e43164.

Shinkai, Y., Yamamoto, Y., Fujiwara, M., Tabata, T., Murayama, T., Hirotsu, T., Ikeda, D.D., Tsunozaki, M., Iino, Y., Bargmann, C.I., et al. (2011). Behavioral choice between conflicting alternatives is regulated by a receptor guanylyl cyclase, GCY-28, and a receptor tyrosine kinase, SCD-2, in AIA interneurons of Caenorhabditis elegans. The Journal of neuroscience *31*, 3007–3015.

Tsalik, E.L., Niacaris, T., Wenick, A.S., Pau, K., Avery, L., and Hobert, O. (2003). LIM homeobox gene-dependent expression of biogenic amine receptors in restricted regions of the C. elegans nervous system. Dev. Biol. *263*, 81–102.

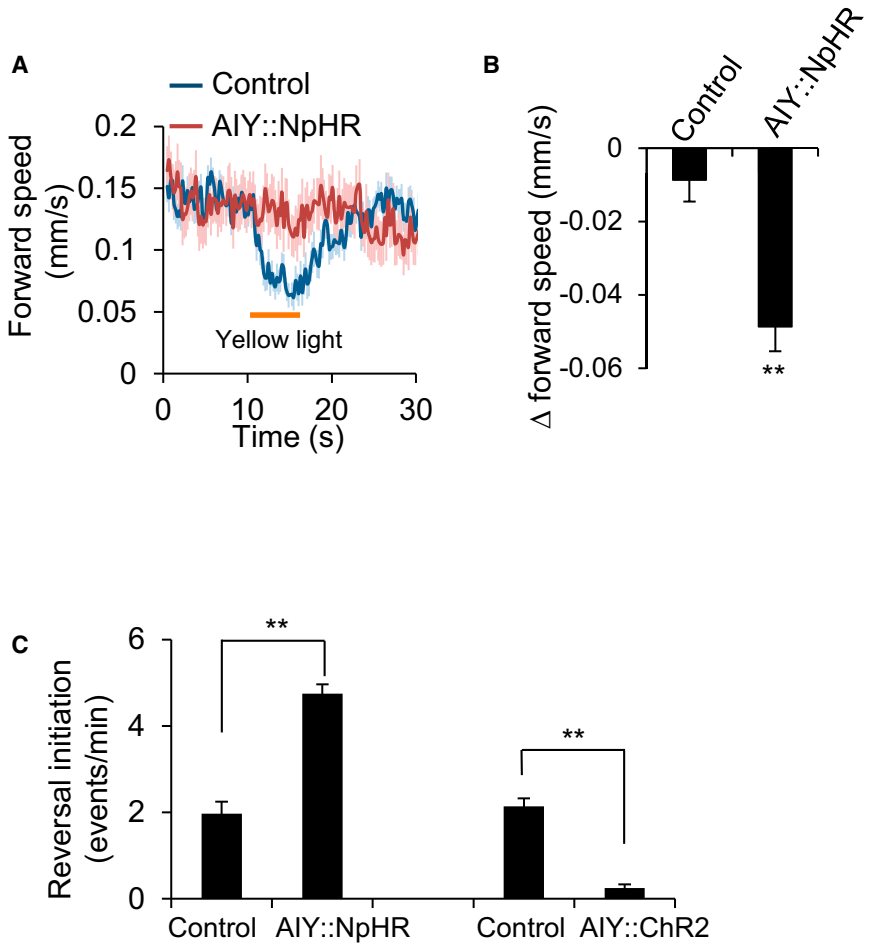

Figure S1. Additional Data on the Effect of AIY::NpHR and AIY::ChR2 on Locomotion Speed and Reversal Initiation, Related to Figure 1

(A and B) AIY::NpHR reduced forward locomotion speed under a low intensity of yellow light (0.3 mW/mm2). Note: when AIY was further inhibited by brighter yellow light (2 mW/mm2), a reversal was triggered (see Figure 1D for details).

(C) Prolonged inhibition and stimulation of AIY by NpHR and ChR2 promotes and suppresses reversal initiation during spontaneous locomotion, respectively. This assay was performed differently from that in Figure 1D, but similarly to that in Figure 1B. Specifically, instead of using 5 s light pulses, we applied prolonged light stimulus (2 min of yellow light at 2 mW/mm2 or blue light at 0.5 mW/mm2) to animals expressing NpHR or ChR2 in AIY, respectively. The number of reversal events was then quantified over 2 min of scoring window. NpHR inhibition of AIY increased the reversal frequency to ~250% of control. This effect is more potent than that obtained with AIY laser ablation, which increased reversal frequency by ~50% (see Figure 1B). Conversely, ChR2 stimulation of AIY nearly eliminated all spontaneous reversal events. Control: nontransgenic siblings. Error bars: SEM $n \geq 10$. **$p < 0.0001$ (t test).

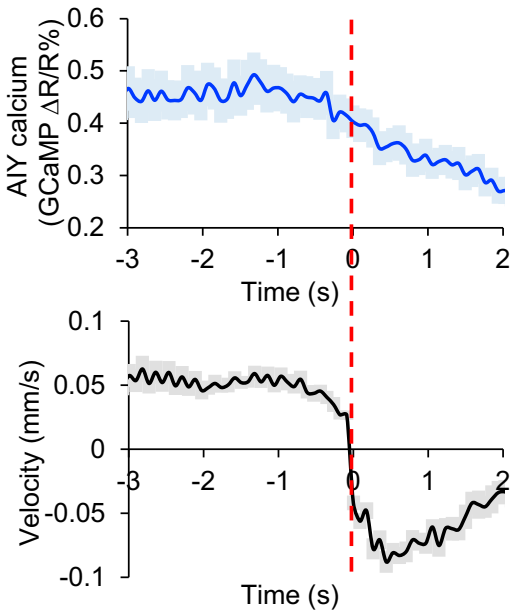

Figure S2. AIY Calcium Level Begins to Decline before the Initiation of Reversals, Related to Figure 2

The segments in calcium and velocity traces surrounding reversal events were analyzed. The dotted line in red marks the time point at which animals initiate reversals. The average calcium level in AIY begins to decline at ~1 s before the initiation of reversals. Shades along the traces represent error bars (SEM). n = 36.

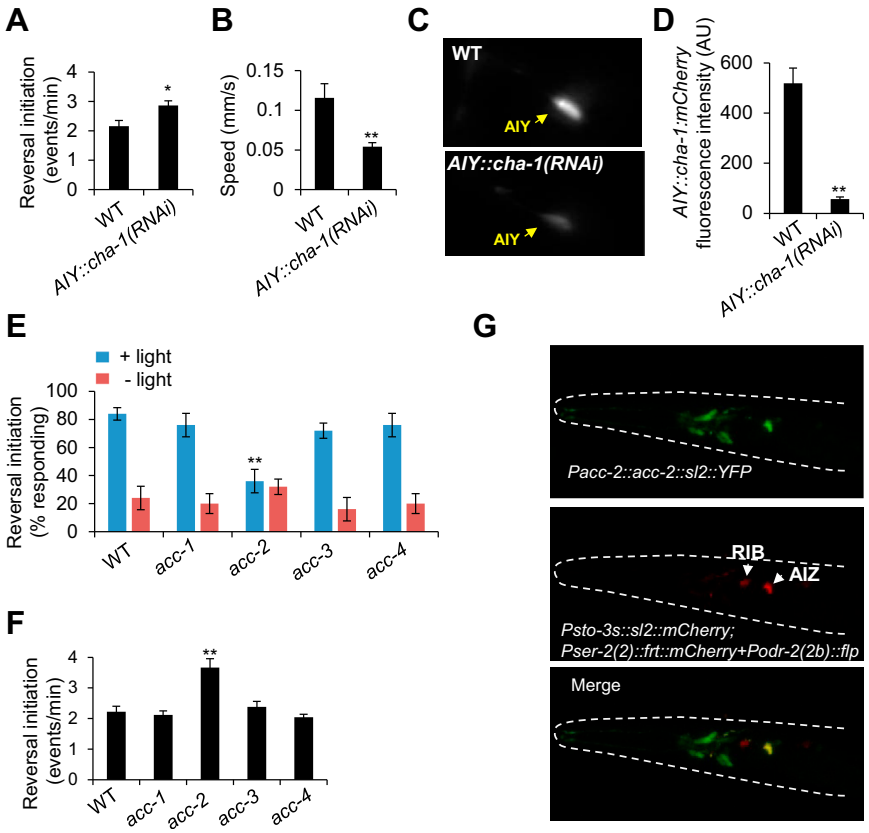

Figure S3. Additional Data on *cha-1* and *acc-2*, Related to Figure 5

(A and B) RNAi of *cha-1* in AIY increases reversal frequency (A), and reduces locomotion speed (B). *cha-1* RNAi were expressed as a transgene specifically in AIY under the *ttx-3 s* promoter. Locomotion behavior was assayed using an automated worm tracking system. Error bars: SEM n ≥ 5. *p < 0.02; **p < 0.0001 (t test).

(C and D) RNAi of *cha-1* knocks down the protein level of CHA-1::mCherry fusion in AIY. To evaluate the effect of *cha-1* RNAi in AIY, we crossed a transgene expressing CHA1::mCherry protein fusion in AIY and then quantified its fluorescence level. *cha-1* RNAi inhibited the protein expression level of CHA-1::mCherry fusion by ~90%. Error bars: SEM n ≥ 32. **p < 0.0001 (t test).

(E) *acc-2,* but not other *acc* genes, is required for AIY to trigger reversals. All genotypes carried a transgene expressing NpHR in AIY under the *ttx-3 s* promoter. The assay was conducted as described in Figure 1D. Yellow light was used to excite NpHR to trigger reversals. No light illumination was used as a control. Error bars: SEM n ≥ 5. **p < 0.0001 (ANOVA with Tukey's HSD test).

(F) *acc-2* mutant worms show an elevated reversal frequency during spontaneous locomotion. Error bars: SEM n ≥ 5. **p < 0.0001 (ANOVA with Tukey's HSD test).

(G) *acc-2* is expressed in AIZ.